UNIVERSITY OF ILLINOIS
URBANA

AERONOMY REPORT NO. 81

D-REGION DIFFERENTIAL-PHASE MEASUREMENTS AND IONIZATION VARIABILITY STUDIES

(NASA-CR-158116) D-REGION DIFFERENTIAL-PHASE MEASUREMENTS AND IONIZATION VARIABILITY STUDIES (Illinois Univ.) 109 p HC A06/MF A01 CSCL 04A
N79-18510
Unclas
G3/46 14091

by
R. M. Weiland
S. A. Bowhill

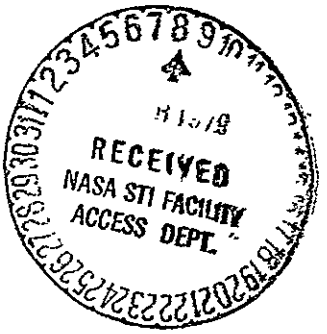

September 1, 1978

Library of Congress ISSN 0568-0581

Supported by
National Aeronautics and Space Administration
Grant NGR 14-005-181

Aeronomy Laboratory
Department of Electrical Engineering
University of Illinois
Urbana, Illinois

CITATION POLICY

The material contained in this report is preliminary information circulated rapidly in the interest of prompt interchange of scientific information and may be later revised on publication in accepted aeronomic journals. It would therefore be appreciated if persons wishing to cite work contained herein would first contact the authors to ascertain if the relevant material is part of a paper published or in process.

UILU-ENG-78-2503

A E R O N O M Y R E P O R T

N O. 81

D-REGION DIFFERENTIAL-PHASE MEASUREMENTS AND IONIZATION VARIABILITY STUDIES

by

R. M. Weiland
S. A. Bowhill

September 1, 1978

Supported by
National Aeronautics
and Space Administration
Grant NGR 14-005-181

Aeronomy Laboratory
Department of Electrical Engineering
University of Illinois
Urbana, Illinois

ABSTRACT

Measurements of electron densities in the *D* region are made by the partial-reflection differential-absorption and differential-phase techniques. The differential-phase data are obtained by a hard-wired phase-measuring system. Electron-density profiles obtained by the two techniques on six occasions are plotted and compared. Electron-density profiles obtained at the same time on 30 occasions during the years 1975 through 1977 are averaged to form a single profile for each technique. The effect of varying the assumed collision-frequency profile on these averaged profiles is studied. It is found that adjusting the assumed collision frequency will bring the averaged electron-density profiles into close agreement, suggesting an error in the collision frequency.

Time series of *D*-region electron-density data obtained by 3.4-minute intervals on six days during the summer of 1977 are examined for wave-like disturbances and tidal oscillations. Short- and long-term oscillations are observed, and the coherency spectra of these oscillations indicate that some of these fluctuations are possibly due to propagating internal gravity waves. The diurnal variations on the six days show an asymmetry about local noon, with a bite-out at noon. Plots of daily electron densities at 72, 76.5, and 81 km for the period of October 1975 through April 1976 show increased variability during the winter months, a clear indication of the occurrence of the winter anomaly at Urbana.

PAGE INTENTIONALLY BLANK

PRECEDING PAGE BLANK NOT FILMED

TABLE OF CONTENTS

ABSTRACT iii
TABLE OF CONTENTS. v
LIST OF FIGURES. vii
1. INTRODUCTION 1
1.1 *D-Region Characteristics*. 1
1.1.1 *The winter anomaly* 1
1.2 *Electron-Density Measurement Techniques* 2
1.2.1 *Differential-absorption technique*. 2
1.2.2 *Differential-phase technique* 3
2. THEORY OF THE PARTIAL-REFLECTION EXPERIMENT. 4
2.1 *Generalized Magnetoionic Theory* 4
2.2 *Differential-Absorption Theory*. 6
2.2.1 *Fresnel reflection model for the differential-absorption experiment* 7
2.2.2 *Volume scattering model for the differential-absorption experiment* 9
2.3 *Differential-Phase Theory* 13
2.3.1 *Fresnel reflection model for the differential-phase experiment* 13
2.3.2 *Volume scattering model for the differential-phase experiment* 14
3. SYSTEM DESCRIPTION 17
3.1 *System Requirements* 17
3.2 *Transmitting Equipment*. 17
3.3 *Receiving Equipment* 19
3.3.1 *Phase detection system* 19
3.3.2 *Phase detection circuitry*. 22
3.4 *Antenna System*. 22
3.5 *Data-Acquisition System* 27
3.5.1 *Sample-and-hold circuitry for collection of simultaneous amplitude and phase data* 28
4. DATA-ANALYSIS TECHNIQUES 32
4.1 *Analysis of Differential-Absorption Data*. 32
4.2 *Analysis of Differential-Phase Data* 33
4.2.1 *Characteristics of the phase-detector returns*. 33

4.2.2 *Data collection and processing programs*. 34
5. PARTIAL-REFLECTION ELECTRON-DENSITY MEASUREMENTS 37
5.1 *Daily Measurements of Electron Densities*. 37
5.2 *Comparison between Differential-Absorption and Differential-Phase Electron-Density Profiles* 47
6. INVESTIGATION OF SHORT- AND MEDIUM-TERM VARIABILITY OF *D*-REGION ELECTRON DENSITIES 59
6.1 *Wave-Like Disturbances in the* D *Region*. 59
6.2 *Diurnal Variations of* D-*Region Electron Densities* 63
7. CONCLUSIONS AND SUGGESTIONS FOR FUTURE WORK. 76
APPENDIX I SEMICONDUCTOR INTEGRAL APPROXIMATIONS BY *BURKE AND HARA* [1963] 77
APPENDIX II ASSUMED COLLISION-FREQUENCY PROFILE 78
APPENDIX III COMPUTER PROGRAMS. 79
REFERENCES 96

LIST OF FIGURES

Figure		Page
3.1	Block diagram of the partial-reflection system.	18
3.2	Phase detection system.	20
3.3	Buffer amplifiers and mixing circuitry.	21
3.4	Block diagram of the phase detector	23
3.5	Schematic of squaring amplifier and zero-crossing detector.	24
3.6	Phase detector circuitry.	25
3.7	Partial-reflection antenna arrays at the Aeronomy Laboratory Field Station	26
3.8	Sample-and-hold circuit with timing logic	29
3.9	Modified channel sequence logic	30
3.10	Sample-and-hold timing.	31
4.1	Histograms showing the distribution of the phase angle $(\phi_x-\phi_o)\Big\vert_{h_2} - (\phi_x-\phi_o)\Big\vert_{h_1}$ for the two altitudes, containing 5000 samples, observed on February 20, 1977 at 12:10. Each small division is 1.5 degrees	35
5.1	Daily plot of electron density at 72, 76.5, and 81 km and Ax/A_O at 81 km for October 1975	38
5.2	Daily plot of electron density at 72, 76.5, and 81 km and Ax/A_O at 81 km for November 1975.	39
5.3	Daily plot of electron density at 72, 76.5, and 81 km and Ax/A_O at 81 km for December 1975.	40
5.4	Daily plot of electron density at 72, 76.5, and 81 km and Ax/A_O at 81 km for January 1976	41
5.5	Daily plot of electron density at 72, 76.5, and 81 km and Ax/A_O at 81 km for February 1976.	42
5.6	Daily plot of electron density at 72, 76.5, and 81 km and Ax/A_O at 81 km for March 1976	43
5.7	Daily plot of electron density at 72, 76.5, and 81 km and Ax/A_O at 81 km for April 1976	44
5.8	76.5-km electron-density monthly means. Error bars indicate $\pm$ 1 standard deviation.	45
5.9	Coefficient of variation of electron densities at 72.0, 76.5, and 81.0 km	46

5.10 Seasonal changes in coefficient of variation (standard deviation/mean) of noon electron densities in three altitude ranges at 44° S [*Gregory and Manson,* 1969b]. 48
5.11 Electron-density profiles obtained by the differential-absorption and differential-phase experiments on November 4, 1975 at 1230 local time 49
5.12 Electron-density profiles obtained by the differential-absorption and differential-phase experiments on November 8, 1975 at 1245 local time 50
5.13 Electron-density profiles obtained by the differential-absorption and differential-phase experiments on March 14, 1976 at 1445 local time 51
5.14 Electron-density profiles obtained by the differential-absorption and differential-phase experiments on October 14, 1976 at 1443 local time 52
5.15 Electron-density profiles obtained by the differential-absorption and differential-phase experiments on October 14, 1976 at 1145 local time 53
5.16 Average of 30 electron-density profiles obtained by the differential-absorption and differential-phase experiments. . . 54
5.17 Average of 30 electron-density profiles obtained by the differential-absorption and differential-phase experiments with the assumed collision-frequency profile multiplied by a factor of 1.25. 55
5.18 Average of 30 electron-density profiles obtained by the differential-absorption and differential-phase experiments with the assumed collision-frequency profile multiplied by a factor of 1.5 56
5.19 Average of 30 electron-density profiles obtained by the differential-absorption and differential-phase experiments with the assumed collision-frequency profile multiplied by a factor of 2.0 57
6.1 Variation of electron density with local time at altitudes 72, 76.5, and 81 km for May 17, 1977. 60
6.2 Spectra of electron-density fluctuations. 62

6.3 Coherency spectra. 64
6.4 Diurnal variation of ionization at 72, 76.5 and 81 km. 69
6.5 Diurnal pressure variation at 75 km. 70
6.6 Day-to-day variation of the diurnal asymmetry. 74

1. INTRODUCTION

1.1 D-*Region Characteristics*

The *D* region is the lower part of the ionosphere, extending from 60 to 90 km. The *D* region is the least understood, and most complex region of the ionosphere. The daytime upper *D*-region ionization is due mainly to photoionization of nitric oxide by solar Lyman-α radiation [*Strobel*, 1971]. Other sources of ionization include solar X-radiation of major *D*-region constituents (O_2 and N_2), galactic cosmic radiation of constituents in the lower *D* region (60 to 70 km), and extreme ultraviolet radiation of metastable molecular oxygen, $O_2(^1\Delta)$ [*Whitten and Poppoff*, 1971]. Also, precipitating energetic electrons may be a significant source of ionization at midlatitudes during geomagnetic storms. The relatively high neutral atmospheric pressure is responsible for the complexity of the ion chemistry in the *D* region. Efficient three-body reactions may occur and large water cluster ions may form. In the lower *D* region the relatively high neutral density allows rapid three-body attachment of electrons to molecular oxygen, which reacts with other neutral gases to form other negative ions.

Because the *D* region is formed mainly by solar radiation, it almost completely disappears at night. The average values of electron densities are higher in the summer months due to a lower solar zenith angle. Electron densities show many variations due to dynamical effects. Variations are observed on many time scales and are caused by many processes. In this work seasonal, day-to-day, diurnal, and shorter time scale variations will be studied.

1.1.1 *The winter anomaly*. There is little day-to-day variation in electron densities measured during the summer months. The electron densities measured during the winter months display a great deal more day-to-day variability. Enhancements of the electron density above 80 km cause abnormally large absorptions of high and medium frequency radio waves on many days during the winter months. This phenomenon has been called the winter anomaly. The winter anomaly is probably the result of several causes, and the relative importance of each on particular days is unknown at this time. The suggested causes of the winter anomaly are summarized by *Sechrist* [1972]. The causes include transport of ionizable minor constituents, the variations in electron loss rate associated with positive-ion composition variations, and the effect of energetic electrons precipitating from the radiation belts after magnetic

storms. Evidence of the winter anomaly in the *D*-region electron densities will be shown in Chapter 5.

1.2 *Electron-Density Measurement Techniques*

The *D* region is particularly difficult to obtain measurements from. It is too high for balloon measurements, and too low for effective satellite measurements. Rocket measurements can be made, but are quite expensive. The best alternative for effective long-term study of the region is the use of ground-based radio-wave probing. Several radio-wave probing methods are used. These include absorption measurements, the ionosonde experiment, the wave-interaction experiment, the incoherent-scatter experiment, and the partial-reflection experiment.

The absorption experiment measures the absorption of a radio wave along an ionospheric path and can be done in several ways. One method is to transmit a pulse vertically, which is nearly totally reflected from the *E* region. The absorption due to the *D* region can thus be determined. The ionosonde experiment sweeps through a range of frequencies, transmitting a signal vertically. The height where total reflection occurs is measured, and the electron density can be calculated. The wave-interaction experiment [*Fejer*, 1955] uses a high-power transmitter to heat the ionosphere. A second transmitter is used in probing the heated region. The heating causes a change in the electron-neutral collision frequency. The probing signal returns for the heated and nonheated ionosphere are then used in calculating the electron density. The incoherent-scatter experiment transmits very high frequency signals upwards and measures the scattered energy from the electrons. This amplitude can be related to the electron density when a calibration measurement is used.

The partial-reflection experiment, which is the subject of this work, is described in the next two sections.

1.2.1 *Differential-absorption technique.* Ordinary and extraordinary mode pulses are alternately transmitted into the ionosphere. These modes are the characteristic modes, which by definition propagate through the medium without a change in polarization, but undergo a different attenuation. As the signals pass through the *D* region, irregularities cause the signals to be partially reflected. By measuring the ratio of the amplitudes of the modal returns as a function of height, an electron-density profile can be calculated.

1.2.2 *Differential-phase technique.* In the differential-phase technique the phase difference between the modal returns is measured as a function of height. The characteristic modes have different phase shifts while propagating through the medium. The phase difference as a function of height can be used to calculate the electron-density profile. This electron-density profile measurement is independent of the differential-absorption measurement.

2. THEORY OF THE PARTIAL-REFLECTION EXPERIMENT

2.1 *Generalized Magnetoionic Theory*

The original partial-reflection experiment performed by *Gardner and Pawsey* [1953] used the Appleton-Hartree formula [*Budden*, 1961] for the refractive index of the medium, which assumed that the collision frequency was directly proportional to the electron velocity. By laboratory experiments, *Phelps and Pack* [1959] established that the collision frequency of an electron in nitrogen gas is proportional to the square of its velocity. *Sen and Wyller* [1960] derived the formula for the refractive index of the medium using a coordinate system with oblique axes, allowing for the harmonic time variation of the radio-wave fields with real factors of cos ωt and sin ωt. *Budden* [1965] derived the same formula using orthogonal axes and a complex time factor $e^{j\omega t}$, giving a simplified approach. The following assumptions are made in their derivation:

1. The medium is a slightly ionized gas.
2. The mass of neutrals is much greater than the mass of electrons.
3. The influence of electron-electron collisions is negligible when compared with the influence of electron-neutral collisions, and collisions are purely elastic.
4. The collision frequency of electrons is proportional to the square of the electron velocity.
5. The electric field energy is negligible compared with the thermal energy so that neutrals and electrons have Maxwell-Boltzmann velocity distributions.

A generalized permittivity tensor is formed in terms of the elements ε_I, ε_{II}, and ε_{III}, which are the permittivities associated with the principal axes defined by the directions of the wave normal and the earth's magnetic field. The permittivity elements are given by:

$$\varepsilon_I = (1 - a) - jb \tag{2.1}$$

$$\varepsilon_{II} = \frac{1}{2}(f - d) + \left(\frac{j}{2}\right)(c - e) \tag{2.2}$$

$$\varepsilon_{III} = [a - \frac{1}{2}(c + e)] + j[b - \frac{1}{2}(f + d)] \tag{2.3}$$

where:

$$a = \frac{\upsilon}{\nu_m^2} \wp_{3/2}\left(\frac{\omega}{\nu_m}\right)$$

$$b = \frac{5}{2}\frac{\omega_o^2}{\omega\nu_m} \wp_{5/2}\left(\frac{\omega}{\nu_m}\right)$$

$$c = \frac{\omega_o^2\,(\omega - \omega_H)}{\omega\nu_m^2} \wp_{3/2}\left(\frac{\omega - \omega_H}{\nu_m}\right)$$

$$d = \frac{5}{2}\frac{\omega_o^2}{\omega\nu_m} \wp_{5/2}\left(\frac{\omega - \omega_H}{\nu_m}\right)$$

$$e = \frac{\omega_o^2\,(\omega + \omega_H)}{\omega\nu_m^2} \wp_{3/2}\left(\frac{\omega + \omega_H}{\nu_m}\right)$$

$$f = \frac{5}{2}\frac{\omega_o^2}{\omega\nu_m} \wp_{5/2}\left(\frac{\omega + \omega_H}{\nu_m}\right)$$

ω = operating frequency

ω_o^2 = plasma frequency $\equiv \frac{Ne^2}{me_o}$

ω_H = angular gyro frequency $\equiv \frac{eB}{m}$

ν_m = electron-neutral collision frequency associated with the most probable electron energy.

N = electron concentration (M^{-3})

e = electron charge = 1.6×10^{-19} C

m = electron mass = 9.1×10^{-31} KG

ε_o = permittivity of free space = 8.85×10^{-12} F/M

B = earth's magnetic field (Webers/M^2).

The semiconductor integrals

$$\wp_p(x) = \frac{1}{p!}\int_o^\infty \frac{u^p\, e^{-u}\, du}{u^2 - x^2}$$

are approximated to within 1% error by the polynomials given by *Burke and Hara* [1963] listed in Appendix I.

The generalized refractive index $n_{o,x}$ is defined as $n_{o,x} = (\mu - jk)$ and is given in terms of the permittivity elements as:

$$n_{o,x} = \left[\frac{A + B \sin^2\theta \pm (B^2 \sin^4\theta - C^2 \cos^2\theta)^{\frac{1}{2}}}{D + E \sin^2\theta} \right]^{\frac{1}{2}} \tag{2.4}$$

where:

$A = 2 \varepsilon_I (\varepsilon_I + \varepsilon_{III})$

$B = \varepsilon_{III} (\varepsilon_I + \varepsilon_{III}) + \varepsilon_{II}^2$

$C = 2\varepsilon_I \varepsilon_{II}$

$D = 2\varepsilon_I$

$E = 2\varepsilon_{III}$

θ = angle between wave normal and the direction of the Earth's magnetic field.

The quasi-longitudinal approximation for small values of θ greatly simplifies the expression:

$$n_{o,x} = \left[\frac{A \pm (-C^2 \cos^2\theta)^{\frac{1}{2}}}{D} \right]^{\frac{1}{2}} \tag{2.5}$$

$$n_{o,x}^2 = 1 - \left[\frac{\omega_o^2 (\omega \pm \omega_L)}{\omega \nu_m^2} \right] \wp_{3/2} \left(\frac{\omega \pm \omega_L}{\nu_m} \right) - j \left(\frac{5 \omega_o^2}{2 \omega \nu_m} \right) \wp_{5/2} \left(\frac{\omega \pm \omega_L}{\nu_m} \right) \tag{2.6}$$

where:

$\omega_L = \omega_H \cos\theta$

The quasi-longitudinal approximation is valid for Urbana, Illinois [*Pimat and Bowhill*, 1968] and is used in daily measurements of electron densities. The full Sen-Wyller expression is used in experimental work on the differential phase system to avoid the slight error introduced by the quasi-longitudinal approximation.

2.2 *Differential-Absorption Theory*

The received amplitude of the partially reflected echo is determined by the absorption losses over the path to the reflecting layer and back, and the loss on reflection. The two-way absorption is given by [*Budden*, 1961]:

$$\exp\left(-2\int_o^h k_{o,x}\,dh\right) \tag{2.7}$$

where $k_{o,x}$ is the absorption coefficient defined as $\frac{\omega}{c}\chi_{o,x}$, where $\chi_{o,x}$ is the imaginary part of the refractive index. The received amplitude is then

$$A_{o,x} \propto R_{o,x} \exp\left(-2\int_o^h k_{o,x}\,dh\right) \tag{2.8}$$

where $R_{o,x}$ is the reflection coefficient. The A_x/A_o ratio can be formed as:

$$\frac{A_x}{A_o} = \frac{|R_x|}{|R_o|}\exp\left[-2\int_o^h (k_x - k_o)\,dh\right] \tag{2.9}$$

Taking the natural logarithm of both sides

$$\ln\left(\frac{A_x}{A_o}\right) = \ln\left(\frac{|R_x|}{|R_o|}\right) - 2\int_o^h (k_x - k_o)\,dh \tag{2.10}$$

If the A_x/A_o ratio is measured experimentally at two closely spaced heights h_1 and h_2, $k_{o,x}$ is approximately constant in that height interval so that the difference in the logarithms of the A_x/A_o ratios can be written as

$$\ln\left(\frac{A_x}{A_o}\right)\Big|_{h_2} - \ln\left(\frac{A_x}{A_o}\right)\Big|_{h_1} =$$

$$\ln\left(\frac{R_x}{R_o}\right)\Big|_{h_2} - \ln\left(\frac{R_x}{R_o}\right)\Big|_{h_1} - 2(k_x - k_o)\Delta h \tag{2.11}$$

where $\Delta h = h_2 - h_1$.

2.2.1 *Fresnel reflection model for the differential-absorption experiment.* The classical partial-reflection theory assumes reflections are due to a sharp discontinuity in the index of refraction. For this Fresnel model, the reflection coefficient is given by

$$R = \frac{n_2 - n_1}{n_2 + n_1} \tag{2.12}$$

Since the observed reflections are weak, the gradient in index of refraction is not large and $n_2 \simeq n_1 \simeq n \simeq 1$, for both modes. The reflection coefficient can be approximated as:

$$R_{o,x} \cong \frac{\delta n_{o,x}}{2n_{o,x}} \tag{2.13}$$

giving us

$$\frac{R_x}{R_o} = \frac{\delta n_x}{n_x} \frac{n_o}{\delta n_o} \tag{2.14}$$

Equation (2.14) is substituted into equation (2.11), with the values for the refractive index given earlier, and the experimentally measured values of A_x/A_o, to obtain electron density values. When using the full Sen-Wyller formula for the refractive indices without the quasi-longitudinal approximation, there is no closed-form expression for the electron concentration. The solution must be obtained by iteration in N. This process requires approximately five minutes for the PDP 15/40 computer to compute an electron density profile.

By using the quasi-longitudinal approximation, the electron density can be solved for explicitly.

The values for n are given by equation (2.6), and $k_{o,x}$ is from the imaginary part of the refractive index, found by expanding (2.6) by the binomial theorem:

$$n_{o,x} =$$

$$\left[1 - \frac{\omega_o^2(\omega \pm \omega_L)}{\omega\nu_m^2} \wp_{3/2}\left(\frac{\omega \pm \omega_L}{\nu_m}\right)\right]^{\frac{1}{2}} - j1/2 \left[\frac{5}{2}\frac{\omega_o^2}{\omega\nu_m} \wp_{5/2}\left(\frac{\omega \pm \omega_L}{\nu_m}\right)\right]$$

$$\cdot \left[1 - \frac{\omega_o^2}{\omega\nu_m}\left(\frac{\omega \pm \omega_L}{\nu_m}\right)\wp_{3/2}\left(\frac{\omega \pm \omega_L}{\nu_m}\right)\right]^{-\frac{1}{2}} + \text{higher order terms} \tag{2.15}$$

since

$$\frac{5}{2}\frac{\omega_o^2}{\omega\nu_m} \wp_{5/2}\left(\frac{\omega \pm \omega_L}{\nu_m}\right) << 1 - \frac{\omega_o^2}{\omega\nu_m}\left(\frac{\omega \pm \omega_L}{\nu_m}\right)\wp_{3/2}\left(\frac{\omega \pm \omega_L}{\nu_m}\right) \simeq 1 \tag{2.16}$$

The higher order terms can be neglected. The real and imaginary parts can be extracted: The real part, $\mu_{o,x}$ is

$$\mu_{o,x} = \left[1 - \frac{\omega_o^2}{\omega\nu_m}\left(\frac{\omega \pm \omega_L}{\nu_m}\right)\wp_{3/2}\left(\frac{\omega \pm \omega_L}{\nu_m}\right)\right]^{\frac{1}{2}} \tag{2.17}$$

The imaginary part, $\chi_{o,x}$ is

$$\chi_{o,x} = \frac{5}{4}\frac{\omega_o^2}{\omega\nu_m} \wp_{5/2}\left(\frac{\omega \pm \omega_L}{\nu_m}\right) \tag{2.18}$$

$$\chi_{o,x} = \frac{5}{4} \frac{Ne^2}{m\varepsilon_o \omega \nu_m} \wp_{5/2}\left(\frac{\omega \pm \omega_L}{\nu_m}\right) \tag{2.19}$$

The real part can again be expanded by the binomial theorem, yielding:

$$\mu_{o,x} = 1 - \frac{\omega_o^2}{2\omega\nu_m}\left(\frac{\omega \pm \omega_L}{\nu_m}\right) \wp_{3/2}\left(\frac{\omega \pm \omega_L}{\nu_m}\right) \tag{2.20}$$

Assuming ν_m is constant across the discontinuity [*Belrose and Burke*, 1964], n^2 is a function of electron density, N alone. Differentiating equation (2.6) with respect to N yields:

$$2n \frac{\delta n}{\delta N} = - \frac{e^2}{m\varepsilon_o \omega \nu_m} \left[\left(\frac{\omega \pm \omega_L}{\nu_m}\right) \wp_{3/2}\left(\frac{\omega \pm \omega_L}{\nu_m}\right) + j \frac{5}{2} \wp_{5/2}\left(\frac{\omega \pm \omega_L}{\nu_m}\right)\right] \tag{2.21}$$

Assuming that $n_o \simeq n_x \simeq 1$ the ratio of reflection coefficients becomes

$$\frac{R_x}{R_o} = \frac{\delta n_x}{\delta n_o} = \frac{\left(\frac{\omega - \omega_L}{\nu_m}\right) \wp_{3/2}\left(\frac{\omega - \omega_L}{\nu_m}\right) + j \frac{5}{2} \wp_{5/2}\left(\frac{\omega - \omega_L}{\nu_m}\right)}{\left(\frac{\omega + \omega_L}{\nu_m}\right) \wp_{3/2}\left(\frac{\omega + \omega_L}{\nu_m}\right) + j \frac{5}{2} \wp_{5/2}\left(\frac{\omega + \omega_L}{\nu_m}\right)} \tag{2.22}$$

$$\frac{|R_x|}{|R_o|} = \left\{ \frac{\left[\left(\frac{\omega - \omega_L}{\nu_m}\right) \wp_{3/2}\left(\frac{\omega - \omega_L}{\nu_m}\right)\right]^2 + \left[\frac{5}{2} \wp_{5/2}\left(\frac{\omega - \omega_L}{\nu_m}\right)\right]^2}{\left[\left(\frac{\omega + \omega_L}{\nu_m}\right) \wp_{3/2}\left(\frac{\omega + \omega_L}{\nu_m}\right)\right]^2 + \left[\frac{5}{2} \wp_{5/2}\left(\frac{\omega + \omega_L}{\nu_m}\right)\right]^2} \right\}^{\frac{1}{2}} \tag{2.23}$$

substituting $k_{o,x} = \frac{\omega}{c} \chi_{o,x}$, with $\chi_{o,x}$ from equation (2.19), into equation (2.11) results in

$$N = \frac{\Delta \ln \frac{|R_x|}{|R_o|} - \Delta \ln \frac{A_x}{A_o}}{\frac{5\,\Delta h e^2}{2\,cm\varepsilon_o \nu_m}\left[\wp_{5/2}\left(\frac{\omega - \omega_L}{\nu_m}\right) - \wp_{5/2}\left(\frac{\omega + \omega_L}{\nu_m}\right)\right]} \tag{2.24}$$

The collision-frequency profile assumed is given in Appendix II, and includes seasonal variations.

2.2.2 *Volume scattering model for the differential-absorption experiment.* The real structure of the irregularities producing partial-reflections is unknown, so there is a great deal of controversy over the type of

reflection model to be used. The first approach was the isolated reflector (Fresnel) model used by *Gardner and Pawsey* [1953], and later by *Belrose and Burke* [1964]. Belrose and Burke found that reflections produced by pulses of different width showed maximums at the same altitude, with more defined minimums displayed with the narrow pulses, and that reflections produced by pulses of different frequencies (40 kHz apart) showed similar structures. They concluded therefore that the reflections were produced by isolated reflectors.

Flood [1968, 1969] developed a model with a pulse width dependence. His volume scattering model assumes that an echo received at time t is from a volume of height $c\tau/2$, where τ is the transmitted pulse width and c is the speed of light. He assumes that the return is a result of a volume of discrete scatterers. The theory allows for the wave to encounter different amounts of absorption in the scattering volume. The Flood model can be written as [*Cohen and Ferraro*, 1973]:

$$\frac{\overline{A_x}^2}{\overline{A_o}^2} = \frac{\hat{K}_o[1 - \exp(-2\hat{K}_x c\tau)]\{[\alpha_x \mathcal{L}_{3/2}(\alpha_x)]^2 + [(5/2)\mathcal{L}_{5/2}(\alpha_x)]^2\}}{\hat{K}_x[1 - \exp(-2\hat{K}_o c\tau)]\{[\alpha_o \mathcal{L}_{3/2}(\alpha_o)]^2 + [(5/2)\mathcal{L}_{5/2}(\alpha_o)]^2\}} \cdot \exp\left[-4\int_o^{cr_B/2}(K_x - K_o)dz\right] \qquad (2.25)$$

where:

$\hat{K}$ is the average value of K within the scattering volume

$K_{x,o} = \{[(5/4)Ne^2]/(m\varepsilon_o c\nu_m)\}\mathcal{L}_{5/2}[(\omega \pm \omega_L)/\nu_m]$

$\alpha_{x,o} = (\omega \pm \omega_L)/[\nu_m(cr/2)]$

$\nu_m(\frac{cr}{2})$ = collision frequency at height $\frac{cr}{2}$

τ = pulse width

r = variable of integration representing time

r_B = $t - \tau$

t = time measured from the leading edge of transmitted pulse to height of interest

Cohen [1971] and *Cohen and Ferraro* [1973] give an improved model which has all the features of the Flood model and also allows the possibility of variation of the reflection coefficient within the scattering volume. The

expression for the Cohen model is:

$$\frac{\overline{A_x^2}}{\overline{A_o^2}} =$$

$$\frac{\int_{r_B}^{r_B+\tau} \left[\frac{N(\frac{cr}{2})}{\omega\, \nu_m(\frac{cr}{2})}\right]^2 \exp\left(-4\int_o^{\frac{cr}{2}} K_x dz\right) \left\{\left[\alpha_x \wp_{3/2}(\alpha_x)\right]^2 + \left[\frac{5}{2}\wp_{5/2}(\alpha_x)\right]^2\right\} dr}{\int_{r_B}^{r_B+\tau} \left[\frac{N(\frac{cr}{2})}{\omega\, \nu_m(\frac{cr}{2})}\right]^2 \exp\left(-4\int_o^{\frac{cr}{2}} K_o dz\right) \left\{\left[\alpha_o \wp_{3/2}(\alpha_o)\right]^2 + \left[\frac{5}{2}\wp_{5/2}(\alpha_o)\right]^2\right\} dr} \quad (2.26)$$

where:

$N(\frac{cr}{2})$ = electron density at height $\frac{cr}{2}$

This reduces to Flood's expression if the electron density and collision frequency are assumed constant over the pulse width.

There has been much dispute as to which model is more appropriate [*Holt*, 1969; *Flood*, 1969], and there is no conclusive evidence to support either model. Studies of the statistical distributions of the amplitudes have been made in an effort to determine the scattering mechanism. It is well known that scattering from a single isolated reflector will result in an amplitude distribution with a Rician probability density. From the central limit theory, scattering from a volume of scatterers would result in an amplitude distribution with a Rayleigh probability density. *Von Biel* [1971] found using this analysis that the amplitude distributions were predominantly Rayleigh below 80 km, and Rician above 80 km. This would predict scattering due to a volume scatterer below 80 km, and scattering from a single reflector above 80 km. *Mathews et al.* [1973] did a slightly more extensive analysis of the amplitude distributions and also predicted volume scattering below 80 km, and single reflector scattering above 80 km. *Newman* [1974] also did an analysis of amplitude distributions and obtained similar results, predicting the scattering mechanism shifting to a single reflector model above 85 km.

Austin and Manson [1969] gave evidence in support of the single reflector model throughout the *D* region. Further work by *Belrose* [1970] lead him

to conclude that in general the reflection process is not uniquely stratified or due to a volume of turbulence, but is a combination of the two. The altitudes where each type of reflection occurs varies from day to day, by season, and with changes in latitude.

The differences between electron densities calculated by the volume-scattering theory and by the single-reflector theory have been computed by *Wratt* [1974]. He found that for a pulse width of 25 μs and an average electron-density profile the difference was at most five percent in the altitude range of 70 to 87.5 km. *Holt* [1969] also investigated the differences in electron densities calculated using both reflection models, and found that with a 25 μs pulse the difference was less than 10 percent throughout the *D* region. In view of the magnitude of the error that may be introduced, the uncertainty of the actual reflection process, and the relative simplicity of the single reflector (Fresnel) model, the single reflector model will be used in this work.

2.3 *Differential-Phase Theory*

The received phase of the partially reflected echo is determined by the phase change while propagating up to the point of reflection and back, and the phase shift due to reflection. The two-way phase shift is given by [*Budden*, 1961]

$$-\frac{2\omega}{c}\int_o^h \mu_{o,x}\, dh \tag{2.27}$$

where $\mu_{o,x}$ is the real part of the refractive index of the medium. Defining ϕ_{Rx} and ϕ_{Ro} as the phase shifts for each mode due to reflection, we have

$$\phi_{o,x} = \phi_{Ro,\ Rx} - \frac{2\omega}{c}\int_o^h \mu_{o,x}\, dh \tag{2.28}$$

where $\phi_{o,x}$ is the received signal phase. The expression for the phase difference between the two received modes is

$$\phi_x - \phi_o = \phi_{Rx} - \phi_{Ro} - \frac{2\omega}{c}\int_o^h (\mu_x - \mu_o)\, dh \tag{2.29}$$

For closely spaced layers the composition will change only slightly so equation (2.29) can be written as a summation over i intervals.

$$\phi_x - \phi_o = \phi_{Rx} - \phi_{Ro} - \frac{2\omega}{c} \sum_{i=o}^{h/\Delta h} (\mu_{x_i} - \mu_{o_i}) \Delta h \tag{2.30}$$

now defining

$$\eta(h) = (\phi_x - \phi_o)\Big|_h \tag{2.31}$$

and writing

$$\Delta\eta = \eta(h_2) - \eta(h_1) \tag{2.32}$$

also defining

$$\beta(h) = \phi_{Rx} - \phi_{Ro} \tag{2.33}$$

and writing

$$\Delta\beta = \beta(h_2) - \beta(h_1) \tag{2.34}$$

the contribution to the total phase shift from a slab of thickness Δh with lower and upper boundaries h_1 and h_2 respectively is

$$\Delta\eta = \Delta\beta - \frac{2\omega}{c} (\mu_x - \mu_o) \Delta h \tag{2.35}$$

2.3.1 *Fresnel reflection model for the differential-phase experiment.* The Fresnel model assumes that the reflections from the ionosphere are due to sharp discontinuities in the index of refraction. The Fresnel reflection coefficient can be written as

$$R_{o,x} = |R_{o,x}| \, e^{j\phi_{R_o,R_x}} \tag{2.36}$$

Thus, the phase shift due to reflection is the argument of the Fresnel reflection coefficient given in equation (2.36).

Electron-density values are obtained by measuring $\Delta\eta$, and calculating $\Delta\beta$ and $\mu_{o,x}$ in equation (2.35). When using the full Sen-Wyller formula without the quasi-longitudinal approximation, N cannot be solved for explicitly, and the solution must be obtained by iteration in N.

The quasi-longitudinal approximation greatly simplifies the expressions so that the explicit solution for electron density can be obtained.

From equation (2.21) the reflection coefficients are

$$R_{o,x} = \frac{\delta n_{o,x}}{2n_{o,x}} = \frac{-\delta N e^2}{4n_{o,x}^2 \, m\varepsilon_o \, \omega\nu_m} \cdot \left[\left(\frac{\omega \pm \omega_L}{\nu_m} \right) \mathcal{C}_{3/2} \left(\frac{\omega \pm \omega_L}{\nu_m} \right) + j \frac{5}{2} \mathcal{C}_{5/2} \left(\frac{\omega \pm \omega_L}{\nu_m} \right) \right] \tag{2.37}$$

with the plus sign for the ordinary mode. The argument of $R_{o,x}$ is the phase shift $\phi_{Ro,\ Rx}$ and is given by

$$\phi_{Ro,\ Rx} = \tan^{-1}\left[\frac{5}{2}\wp_{5/2}\left(\frac{\omega \pm \omega_L}{\nu_m}\right) \Big/ \left(\frac{\omega \pm \omega_L}{\nu_m}\right)\wp_{3/2}\left(\frac{\omega \pm \omega_L}{\nu_m}\right)\right] \tag{2.38}$$

with the plus sign for the ordinary mode. The expressions for $\phi_{Ro,\ Rx}$ are dependent on collision frequency and not on electron concentration.

The real part of the refractive index, $\mu_{o,x}$ is given by equation (2.20), and from this we obtain

$$\mu_x - \mu_o = \frac{Ne^2}{2\omega\, m\varepsilon_o\, \nu_m} \cdot \left[\frac{\omega - \omega_L}{\nu_m}\wp_{3/2}\left(\frac{\omega - \omega_L}{\nu_m}\right) - \frac{\omega + \omega_L}{\nu_m}\wp_{3/2}\left(\frac{\omega + \omega_L}{\nu_m}\right)\right] \tag{2.39}$$

Substituting into equation (2.35) gives us an expression for the electron density.

$$N = \frac{\Delta\beta - \Delta\eta}{\frac{e^2\Delta h}{cm\varepsilon_o\,\nu_m}\left[\frac{\omega - \omega_L}{\nu_m}\wp_{3/2}\left(\frac{\omega - \omega_L}{\nu_m}\right) - \frac{\omega + \omega_L}{\nu_m}\wp_{3/2}\left(\frac{\omega + \omega_L}{\nu_m}\right)\right]} \tag{2.40}$$

A priori knowledge of the collision frequency must be assumed. The profile used is given in Appendix II.

2.3.2 *Volume scattering model for the differential-phase experiment.* As discussed in section 2.2.2, the actual mechanism of reflection in the *D* region is unknown. The single-reflector theory for the directly measured differential-phase experiment was given by *Connolly* [1971]. A volume theory following the same basic assumptions as the volume differential-absorption experiment of *Cohen* [1971] was derived by *Newman* [1974]. He derived an expression for $E[\Delta\phi_s]$, the expected value of the phase angle contributed by the reflection coefficients:

$$E[\Delta\phi_s] = \frac{\int_{r_B}^{r_B+\tau} \frac{5\xi \langle|a|^2\rangle}{2\tau} \left[\frac{\beta N(\frac{cr}{2})\, e^2}{\varepsilon_o m\omega\, \nu_m(\frac{cr}{2})}\right]^2}{\int_{r_B}^{r_B+\tau} \frac{\xi \langle|a|^2\rangle}{\tau} \left[\frac{\beta N(\frac{cr}{2})\, e^2}{\varepsilon_o m\omega\, \nu_m(\frac{cr}{2})}\right]^2}$$

$$\cdot \frac{\left[\alpha_o \mathcal{L}_{3/2}(\alpha_o)\, \mathcal{L}_{5/2}(\alpha_x) - \alpha_x \mathcal{L}_{3/2}(\alpha_x)\, \mathcal{L}_{5/2}(\alpha_o)\right]}{\left[\alpha_x\alpha_o \mathcal{L}_{3/2}(\alpha_x)\, \mathcal{L}_{3/2}(\alpha_o) + \frac{25}{4} \mathcal{L}_{5/2}(\alpha_x)\, \mathcal{L}_{5/2}(\alpha_o)\right]}$$

$$\cdot \frac{\exp\left\{\frac{-5e^2}{2m\varepsilon_o c}\int_o^{\frac{cr}{2}} \frac{N(z)}{\nu_m(z)}\left[\mathcal{L}_{5/2}(\alpha_x) + \mathcal{L}_{5/2}(\alpha_o)\right] dz\right\} dr}{\exp\left\{\frac{-5e^2}{2m\varepsilon_o c}\int_o^{\frac{cr}{2}} \frac{N(z)}{\nu_m(z)}\left[\mathcal{L}_{5/2}(\alpha_x) + \mathcal{L}_{5/2}(\alpha_o)\right] dz\right\} dr} \qquad (2.41)$$

where:

$N(\frac{cr}{2})$ = electron density at $\frac{cr}{2}$

$\nu_m(\frac{cr}{2})$ = collision frequency at $\frac{cr}{2}$

$\alpha_{o,x}$ = $(\omega \pm \omega_L)/[\nu_m(cr/2)]$

r = variable of integration representing time

r_B = $t - \tau$

t = time measured from the leading edge of the transmitted pulse to the height of interest

a = complex random variable geometric scale factor

ξ = average number of irregularities within the scattering volume

β = $\Delta N/N$ a constant dependence of the irregularities on the background electron density.

The total expected phase difference is then given by

$$E[\Delta\phi] = \frac{-2\omega}{c}\int_o^{h_c} (\mu_x - \mu_o)dz + E[\phi_s] \qquad (2.42)$$

where h_c is the center of the scattering volume. Newman did an analysis of the differences in electron-density calculations for the single-scatterer and volume-scatterer models. He found for a 25 μs pulse width that the

difference was less than one percent in the altitude region above 70 km. For this reason, and due to uncertainties in the actual reflection mechanism, the more easily applied single reflector model will be used in this work for differential-phase electron-density calculations as well.

3. SYSTEM DESCRIPTION

3.1 *System Requirements*

The partial-reflection system is located at the Aeronomy Laboratory Field Station near Urbana, Illinois (geographic coordinates: 40° 10' 10" N, 88° 09' 36" W). A diagram of the system is shown in Figure 3.1.

The nature of the signals reflected from *D*-region irregularities put strong requirements on the elements of the system. The reflection coefficients are quite small in the *D* region at the frequency in use, and are of the order of 10^{-3} at the upper *D* region and 10^{-6} in the lower *D* region [*da Silva and Bowhill*, 1974]. While the ordinary mode pulse propagates through the region, the extraordinary mode pulse is strongly attenuated as it passes through ionized layers. At 60 km the reflections from both modes are just above the noise level. The ordinary mode returns steadily grow stronger with altitude of reflection until they saturate the receiver (saturation with full system sensitivity normally occurs at around 85 km), due to the reflection coefficient increasing with altitude. The extraordinary mode returns increase with reflection altitude until they peak at around 75 km, and then at higher altitudes the attenuation effect of the extraordinary mode becomes dominant causing a decrease in the amplitude of the returns with reflection altitude until they again reach the noise level near 90 km. Also, the fading of returns from each height causes the signals to undergo even more amplitude variation. These characteristics of the returns set the requirements for system gain and linearity.

The system can be broken down into four sections; the transmitter, the receiver, the antenna, and the data-acquisition section.

3.2 *Transmitting Equipment*

A large transmitted signal power is required to provide usable returns at lower altitudes. The characteristics of the transmitter in use are:

Peak power: 50 kW

Frequency: 2.66 MHz

Pulse width: 23 μs

Output impedance: 50 OHM, unbalanced

Pulse repetition rate: 2.5 double-pulse frames/s or 2.5 four-pulse frames/s.

The transmitter is a multistage tube type, and is fully described by *Henry* [1966] and by *Pirnat and Bowhill* [1968].

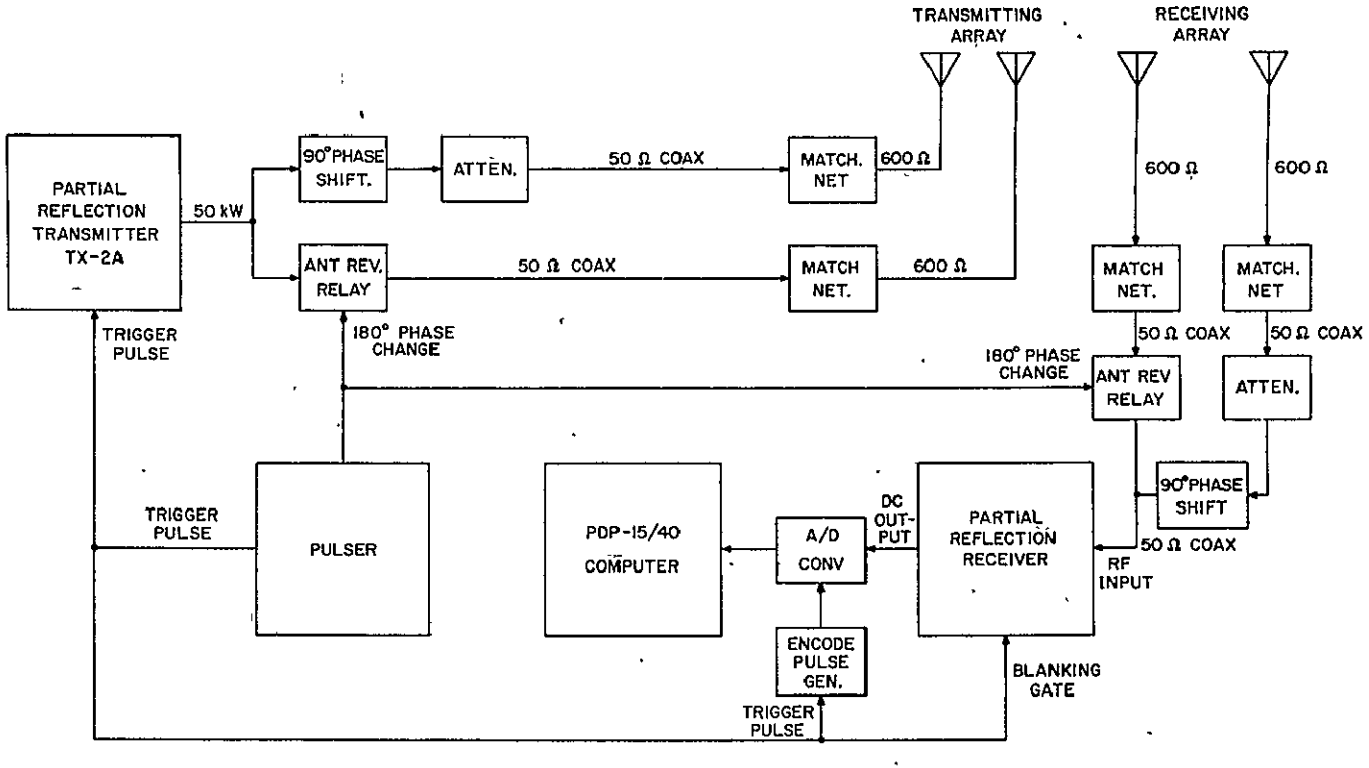

Figure 3.1. Block diagram of the partial-reflection system.

3.3 *Receiving Equipment*

Due to the fact that signal amplitudes must be accurately measured over a 50 dB return signal range, an extremely linear receiver must be used. The original partial-reflection receiver [*Henry*, 1966] had a total range of 20 dB for 1 dB deviation in linearity. The detector circuit was modified later [Henry in *Edwards*, 1973a] to achieve a total range of 55 dB for 1 dB deviation in linearity. The characteristics of the receiver are listed below:

Center frequency: 2.66 MHz

Noise figure: 3 dB

Bandwidth: 40 kHz (between -3 dB points)

Recovery time: 200 μs after removal of 0.1 V RMS input

Gain variation: 3 dB max, 15° to 35° C

RF input impedance: 50 OHM, unbalanced

Output impedance: 10 K OHM, unbalanced

Output response: dc to 50 kHz, 10 V max

Linearity: 55 dB for 1 dB deviation

3.3.1 *Phase detection system.* This section is a description of the phase detector hardware designed by *Abert* [1975]. To establish the proper phase reference, the transmit frequency is mixed down in the same manner as the return wave. Figure 3.2 is a block diagram showing how the phase reference signal at 455 kHz is derived from the partial-reflection system. Using this derived reference signal assures that both received return signals and reference signal are equally affected by any possible oscillator drift, so as to cancel when their difference is taken in the phase detector.

The mixers used to derive the reference signal are Hewlett-Packard 1053 A ring-diode balanced mexers, with a dynamic range of 105 dB. Low-pass filters are added after each mixer to attenuate the unwanted mixer products by 40 dB. Isolation amplifiers are inserted between the RF and IF oscillators and their respective mixer inputs to minimize interaction. The RF local oscillator isolation amplifier has an imput impedance of 3 K OHMS, output impedance of 50 OHMS and a voltage gain of 2.5. The IF local oscillator isolation amplifier has an input impedance of 10 K OHMS, an output impedance of 50 OHMS, and a voltage gain of 1.0. Figure 3.3 shows the circuitry of the isolation amplifiers, mixers, and filters used in deriving the reference signal.

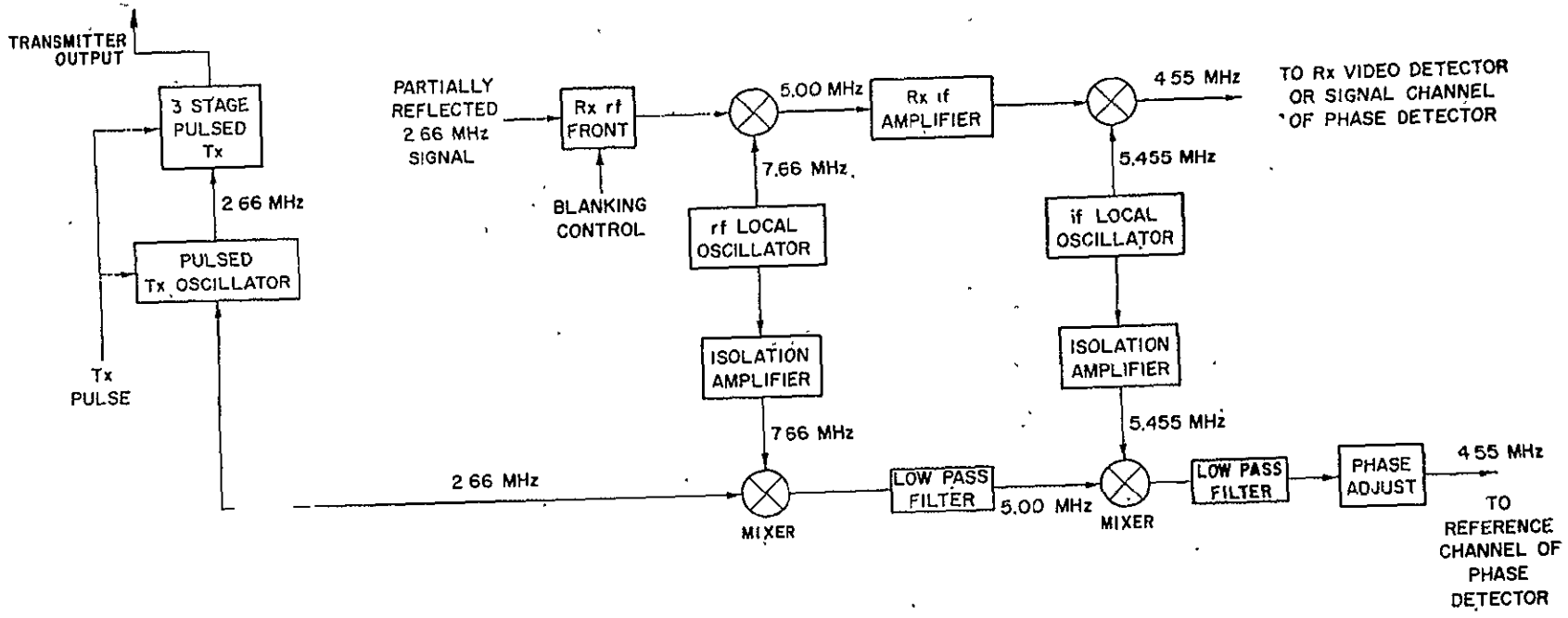

Figure 3.2 Phase detection system.

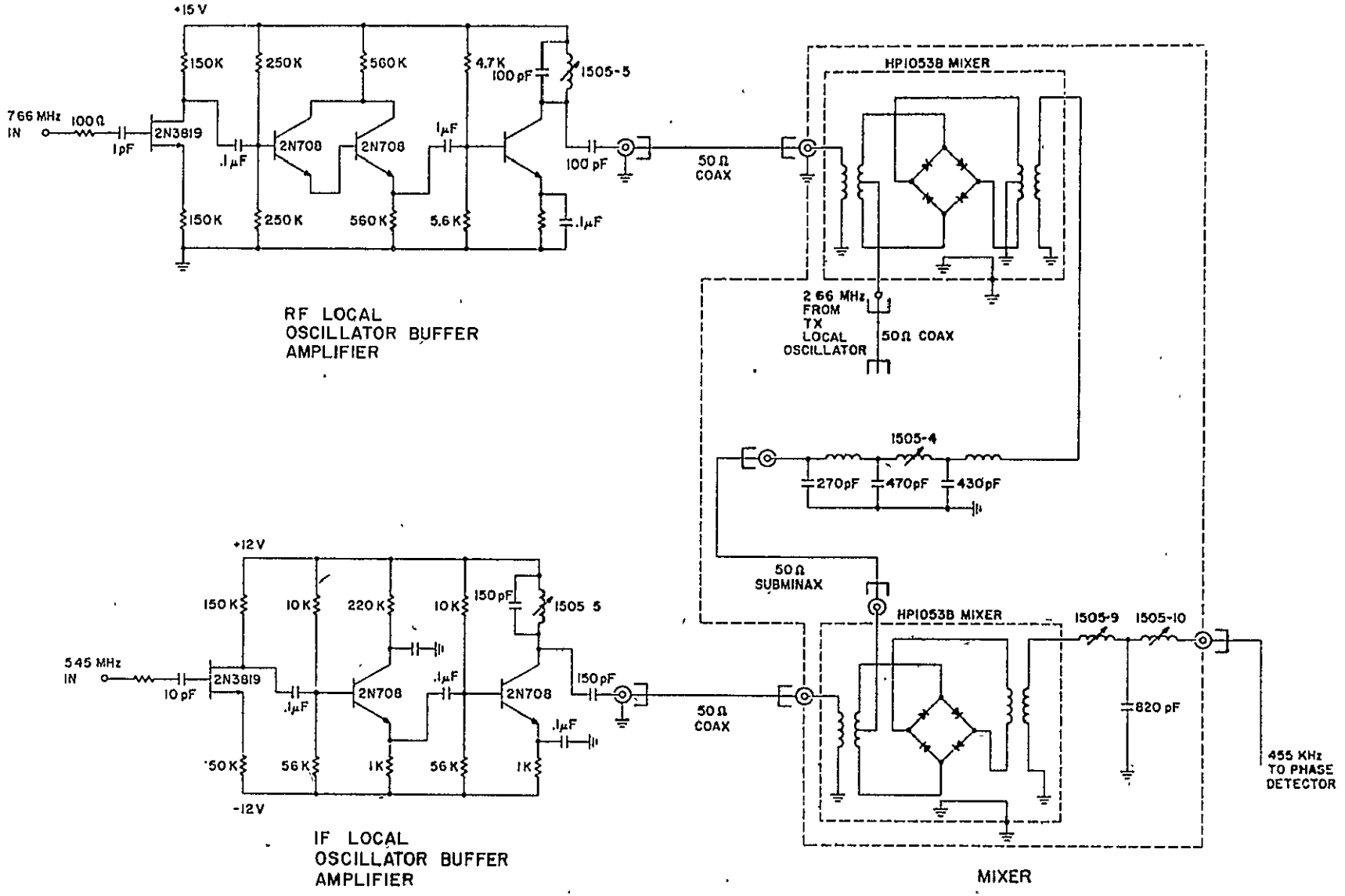

Figure 3.3 Buffer amplifiers and mixing circuitry.

3.3.2 *Phase detection circuitry.* The phase detector must be capable of working over the large range of amplitudes of returned signals. It must also be capable of measuring the range of phase differences likely to be encountered. The expected phase difference has been calculated from an electron-density profile obtained by rocket data [Abert in *Edwards,* 1974b]. This expected phase difference under active sun conditions reaches 180 degrees near 83 km and exceeds 360 degrees at nearly 85 km. Under quiet sun conditions, the expected phase difference is below 360 degrees up to 90 km. The detector then should have a range of 360 degrees. A phase detector used previously by another group [*Mathews and Connally,* 1972] used a NAND gate as a phase comparator, which has a useful range of 180 degrees, leading to ambiguous results at higher altitudes.

The phase detector in use is shown in the block diagram of Figure 3.4. The 455 kHz signal from the receiver IF and the 455 kHz reference signal first go through a hard limiter and then a zero-crossing detector to produce a square wave output that is independent of input amplitude over a range of 45 dB. Figure 3.5 is a schematic of the squaring amplifier and zero-crossing detector for one of the two channels.

The phase comparator is a Motorola MC 4044 integrated circuit comparator which contains sequential logic circuitry capable of measuring phase differences over a range of $\pm$ 360 degrees. The circuit of the phase detector is shown in Figure 3.6. The circuit responds only to transitions and is not sensitive to waveform amplitude or duty cycle. The output of the comparator varies linearly from 0.75 to 2.25 volts as the phase difference varies from -360 degrees to +360 degrees. An amplifier stage with level shifting was added to make the detector output compatible with the existing analog-to-digital converter. This stage provides an output voltage range of 0 to 1 volt for the phase difference range of -360 degrees to +360 degrees. The output amplifier frequency response is flat out to 100 kHz, which is the sampling rate of the analog-to-digital converter. A bandstop filter is added to the output to eliminate any frequency component at 455 kHz.

3.4 *Antenna System*

The partial-reflection antenna system consists of two separate square dipole arrays, each made up of 60 half-wave dipoles. One array is used for transmitting and the other is used for receiving, to eliminate the need for a transmit-receive switch. Figure 3.7 is a diagram of the arrays. The cal-

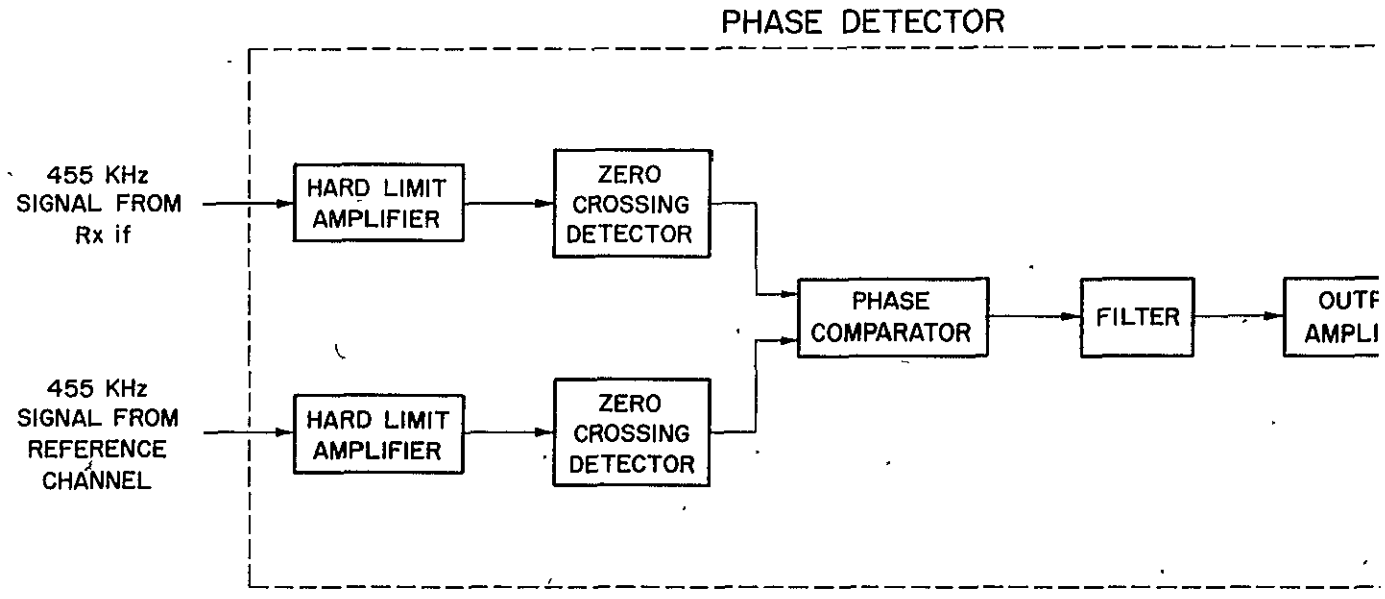

Figure 3.4 Block diagram of the phase detector.

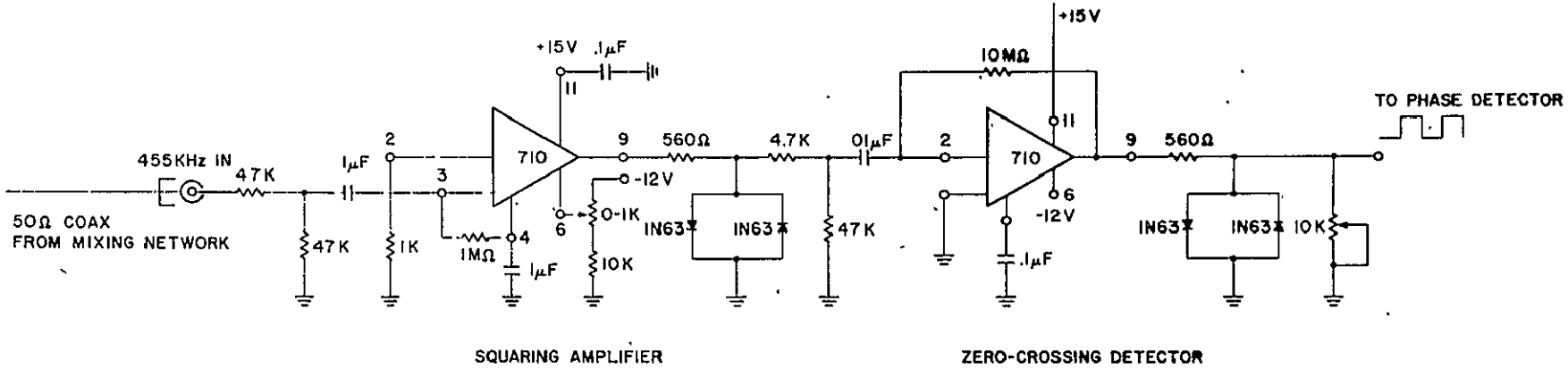

Figure 3.5 Schematic of squaring amplifier and zero-crossing detector.

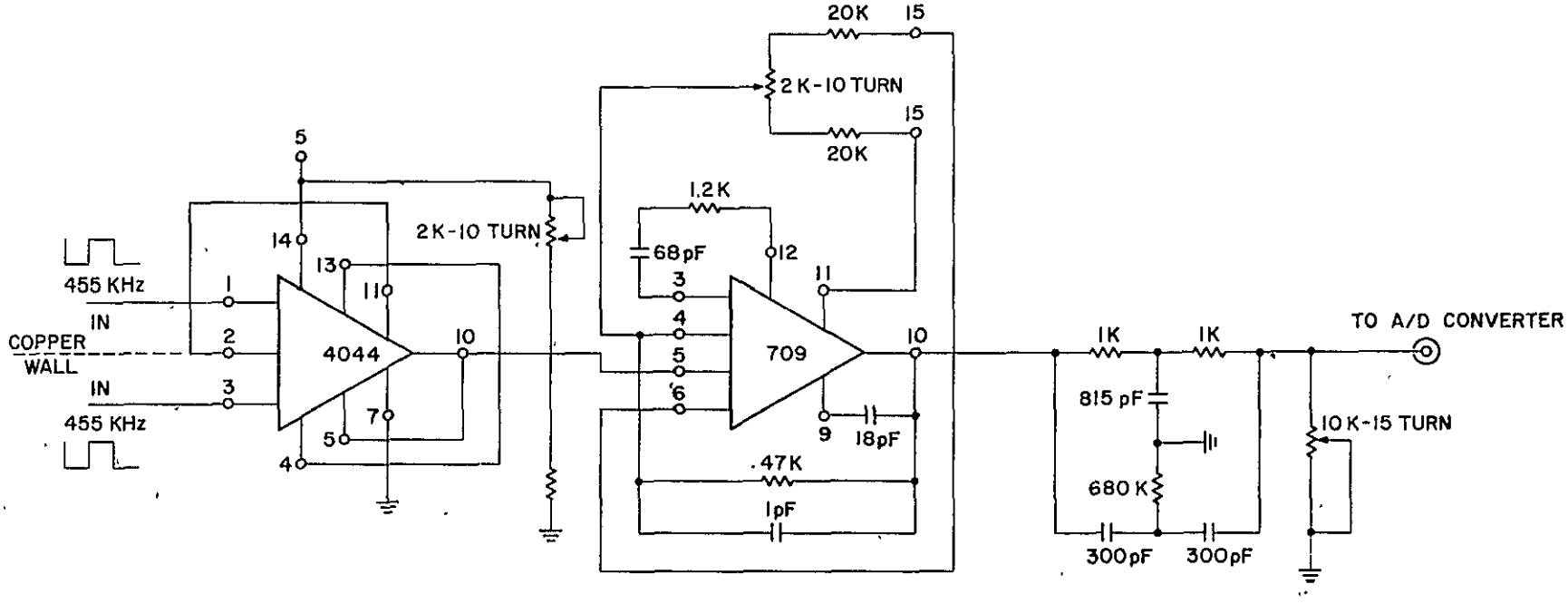

Figure 3.6 Phase detector circuitry.

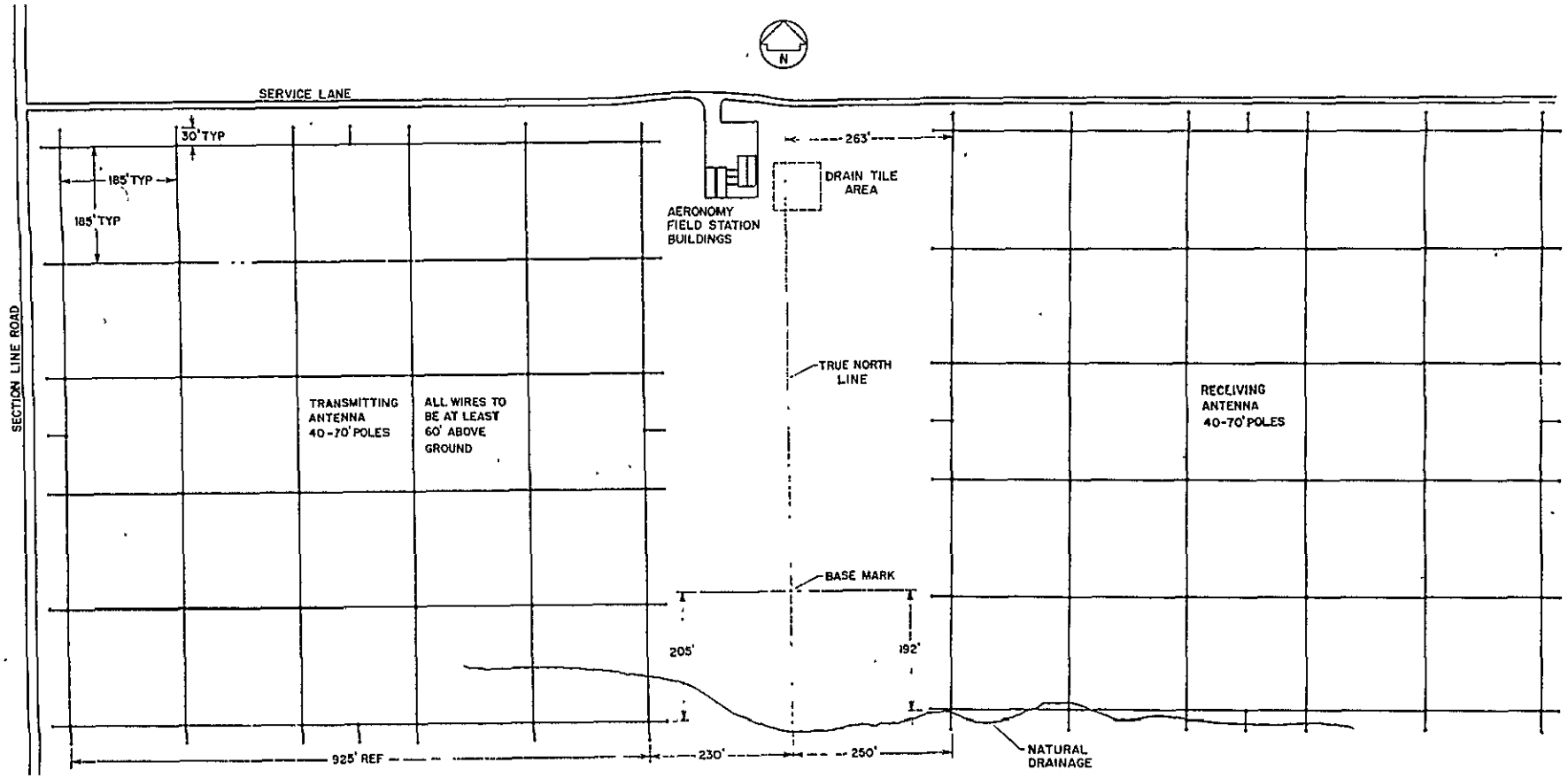

Figure 3.7 Partial-reflection antenna arrays at the Aeronomy Laboratory Field Station.

culated gain of each array is 22 dB, and the calculated beamwidth is 14 degrees. The north-south and east-west set of dipoles are matched to separate feeders and brought into the Field Station building. The polarization, for either array can be switched inside the building to left-hand or right-hand circular polarization, or north-south or east-west linear polarization. Attenuators and phase shifters are inserted in each feeder so that the ellipticity of each array can be adjusted for the maximum rejection of the opposite circular polarization, as measured from ionospheric returns.

The procedure for adjusting the antenna polarizations is given in *Edwards* [1973a]. The computer program POLCHK was written to utilize the digital input/output interface to the PDP 15/40 computer to ease the task of measuring the rejection of the opposite mode of circular polarization. The program switches a manual attenuator into the receiver antenna input line during the ordinary mode return. This attenuator can be switched manually in 1 dB steps to bring the ordinary mode return amplitude down to the extraordinary mode return amplitude, as displayed on the A-scope. Measurements are taken from a sharp discontinuity in the *E* or *F* region. Thus, the rejection ratio of each antenna system can be determined. The program includes the provision for setting the digital attenuator of the system to any desired attenuation up to 63 dB, to prevent saturation of the receiver from these strong signals. To change the attenuator setting, data switch 17 depressed momentarily and the desired attenuation is typed into the teletype followed by a carraige return. The program has been added to the main partial-reflection program tape, and all of its subroutines (INTER, INPADF, SYNC, OUT) are included in the library file on that tape. To run the program, .DAT slots -4 and -5 are assigned to the tape, and the linking loader is called to load and execute POLCHK. A listing of the program and its subroutines is given in Appendix III.

3.5 *Data-Acquisition System*

A Digital Equipment Corporation PDP 15/40 digital computer is used for data acquisition and processing. It is a background-foreground system with 18-bit words and 32 k of core memory. Peripherals include two disk pairs, four DECtape drives, a paper punch and reader, a cathode-ray-tube display terminal, and a General Electric Terminet-1200 high-speed teletype. A Hewlett-Packard 5610 A analog-to-digital converter is used to digitize data. It has a multiplexer so that any one of 16 channels can be sampled at a time, and has a 10-bit word output, in two's complement form. Thus, the 0 to 1

volt input range in use corresponds to an A/D output of from 0 to 512 base 10. Conversion of data in the free run mode occurs at a 100 kHz rate, corresponding to an apparent height resolution of 1.5 km, for a single channel input. A complete description of the computer system can be found by *Birley and Sechrist* [1971], and *Bean and Bowhill* [1973].

3.5.1 *Sample-and-hold circuitry for collection of simultaneous amplitude and phase data:* A circuit has been built to allow simultaneous amplitude and phase data collection. The circuit shown in Figure 3.8 contains two sample-and-hold circuits, and the associated timing circuitry. The Hewlett-Packard 5610 A analog-to-digital converter has a conversion time of 10 μs. It is used in the free run mode, so a sample is converted every 1.5 km of apparent height. For simultaneous operation, the external sample-and-hold circuits will be triggered every 20 μs (or 3 km of apparent height), in the desired height region. These two inputs will be held on the A/D input channels 0 and 1. With the A/D converter in the free run mode, an encode command, given in the height region 45 to 90 km, causes samples to be converted every 10 μs. The channel sequence logic, which externally selects which of the 16 channel inputs on the A/D is to be sampled [Hess in *Edwards*, 1975a; *Hess and Bowhill*, 1976] was modified to correctly sequence through the two input channels. Figure 3.9 shows the inputs added to the channel sequence logic. The reset to channel 0 assures that collection will start with amplitude data at the first measurement. The data collection program will sort out the sequentially converted samples for the processing programs.

The sample-and-hold command and channel sequencing signals are derived from the data-ready flag of the A/D converter. Therefore, the circuit is active only during the encode command period. A timing diagram is shown in Figure 3.10. The chain of monostable multivibrators is used to obtain a 1-μs-wide pulse delayed from the data-ready flag by 4.5 μs. A J-K flip-flop is used to divide the number of delayed pulses to provide a single pulse every 20 μs. The flip-flop is preset to the 1 state by a transmit time pulse, so that the first data-ready flag will be followed by a sample command during the next conversion cycle, and conversion of the inputs will occur during the second next two conversion cycles. To obtain the correct height for the samples, the encode signal must be given to the A/D converter 14 μs earlier than in the present system (which starts conversion 2 μs after the encode command), so that the first sample will occur at the desired apparent height of 45 km.

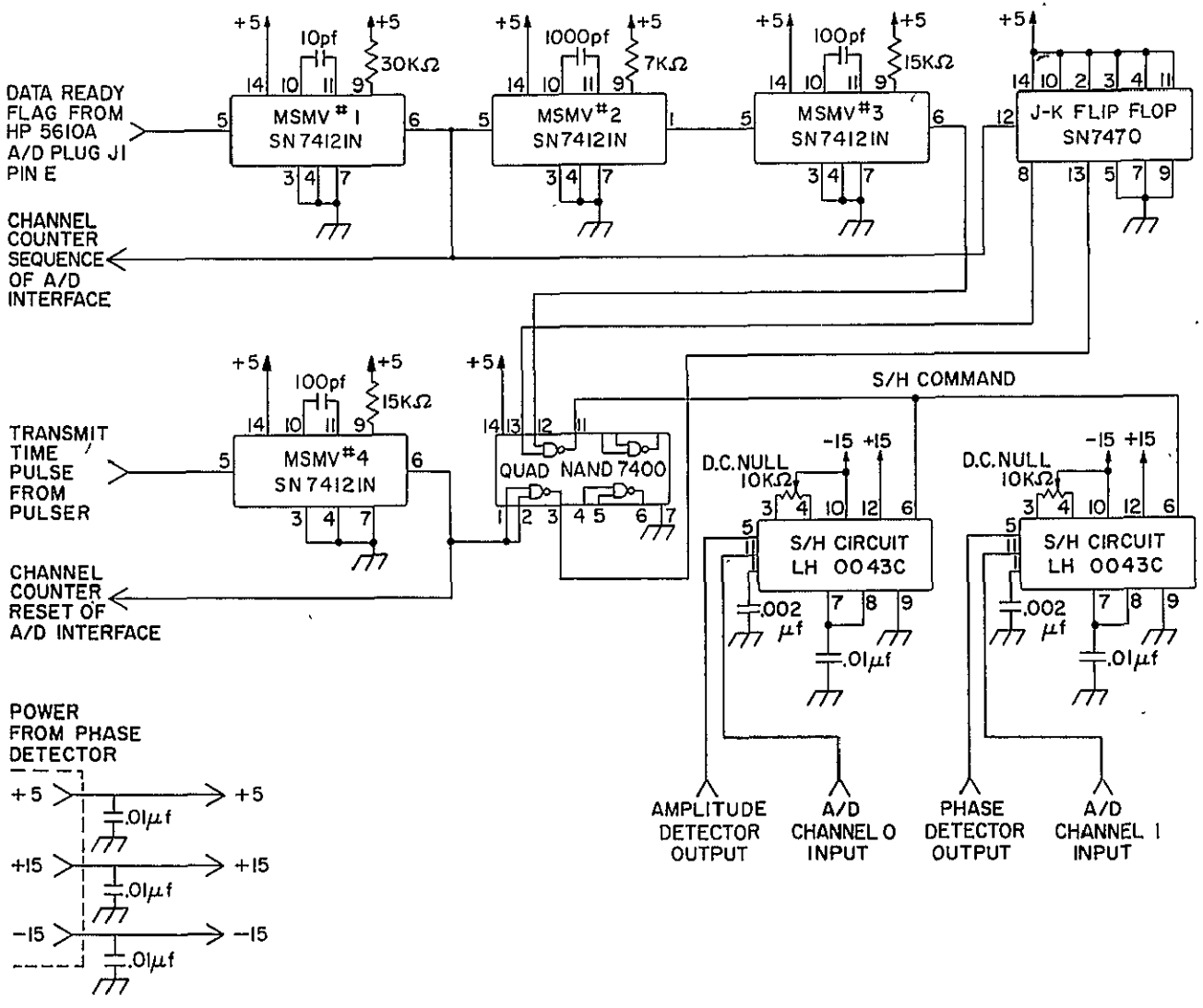

Figure 3.8 Sample-and-hold circuit with timing logic.

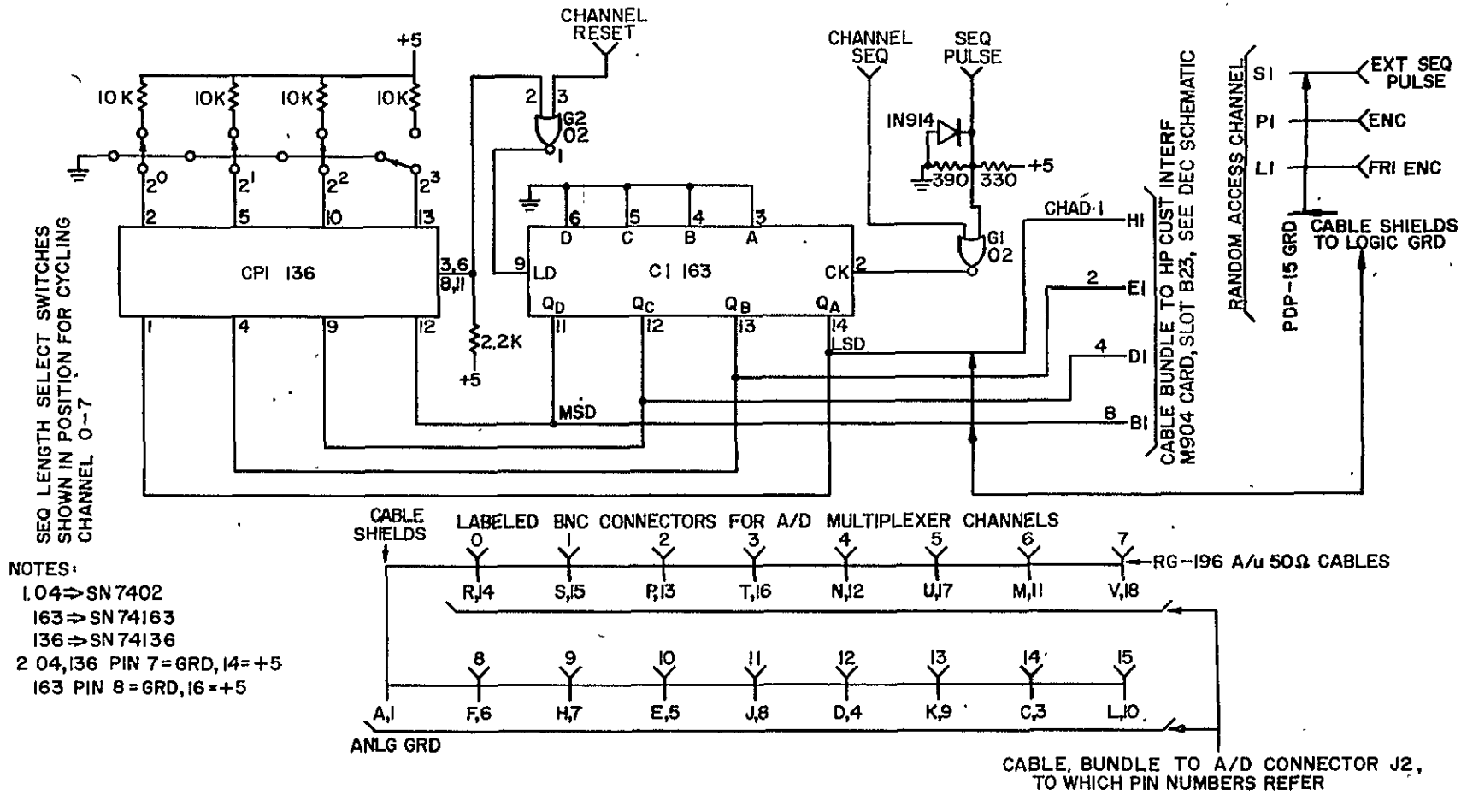

Figure 3.9 Modified channel sequence logic.

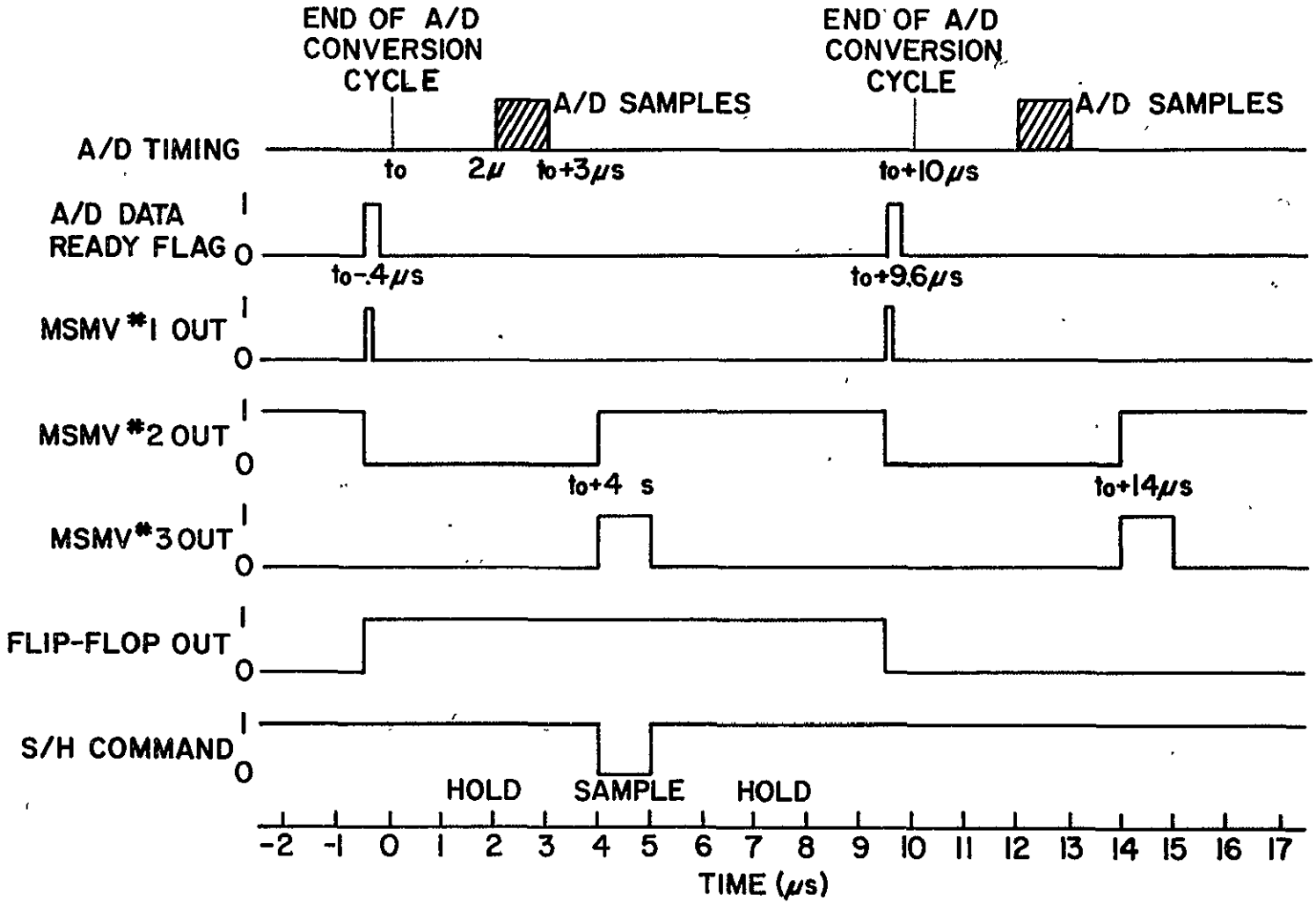

Figure 3.10 Sample-and-hold timing.

4. DATA-ANALYSIS TECHNIQUES

4.1 *Analysis of Differential-Absorption Data*

Differential-absorption data are collected on a regular basis at the Aeronomy Laboratory Field Station. Data are collected daily near noon during the months of October through April, and twice weekly during the summer months. These data are being used in studies of day-to-day *D*-region electron-density variability associated with the 'winter anomaly'. For these studies, a one-hour collection routine is used to obtain a value of electron density at 72, 76.5, and 81 km, and a value of A_x/A_o at 81 km. These data are plotted and published semiannually [*Edwards*, 1973a,b, 1974a,b, 1975a,b, 1976a,b, 1977a,b, 1978]. The collection routine summarized here is described in detail by *Bean and Bowhill* [1973].

The transmitted frame consists of a pair of pulses, an ordinary mode pulse, followed 33 ms later by an extraordinary mode pulse. Data are digitized by 1.5 km intervals over the height range of 45 to 90 km, and collected in 3.4-minute files. The data from the lowest five altitudes, from 45 to 51 km (where no appreciable electron density exists, and hence no returns are expected) are used to estimate the noise level during the collection of that set of data. A noise threshold is determined from the previously collected 3.4-minute file of noise samples (the first file uses noise data from 45 samples taken initially). The square of this noise threshold is multiplied by five and compared with the sum of the squares of the five low-altitude noise samples from each data set. If the noise of either the ordinary or the extraordinary mode is greater than the noise threshold, both sets of data are rejected. A running count is kept of the number of frames rejected, to provide an indication of the actual number of frames of data used in each file. The noise power obtained from the noise samples is then subtracted from the data returns. Data digitized in the height range of 52.5 through 58.5 km are not retained for further processing.

Files of 513 samples (or 3.4 minutes) are collected with 0 dB, 10 dB, and 25 dB of attenuation inserted ahead of the receiver. An electron-density profile is calculated for each file. This group of three files is merged to obtain a single electron-density profile, by receiver saturation criterion. The receiver saturates at one volt output, so any data above this amplitude is assumed to have saturated the receiver. A running count is kept of the number of saturations at each altitude. If more than ten samples saturated

the receiver at a particular altitude, the data at that altitude are then taken from the next higher attenuation file to form the merged file.

Five of these merged files are collected, requiring about one hour. The median value of electron density is found at each altitude from the five merged files, and a final electron-density profile is printed. Averages are calculated for 3-km-wide slabs centered at 72, 76.5, and 81 km. This is done by averaging the electron-density values from two adjacent altitudes. For example, the 72-km electron density is obtained by averaging the values from 70.5 and 72 km. Since the electron density at 70.5 is obtained from

$$\ln(A_x/A_o)\Big|_{72\text{ km}} - \ln(A_x/A_o)\Big|_{70.5\text{ km}} \tag{4.1}$$

and the 72-km electron density is obtained from

$$\ln(A_x/A_o)\Big|_{73.5\text{ km}} - \ln(A_x/A_o)\Big|_{72\text{ km}} \tag{4.2}$$

The average of these two is representative for 72 km. These average values at 72, 76.5, and 81 km are plotted for further study, as is done in Chapter 5.

4.2 *Analysis of Differential-Phase Data*

This section deals with the characteristics of the phase detector returns, and the methods used in collection and processing of the data.

4.2.1 *Characteristics of the phase-detector returns.* The output of the phase detector is a phase angle with respect to the system reference oscillator. The phase angles measured have an ambiguity of $2n\pi$ (n an integer), so that the angles measured at two adjacent altitudes may be written as

$$\phi_{x_1} + 2a\pi \tag{4.3}$$

$$\phi_{o_1} + 2b\pi \tag{4.4}$$

$$\phi_{x_2} + 2c\pi \tag{4.5}$$

$$\phi_{o_2} + 2d\pi \tag{4.6}$$

x, o denoting mode; numerical subscript denoting altitude; a, b, c, d are arbitrary integers.

Consider from equations (2.31) and (2.32)

$$\Delta\eta = (\phi_{x_2} - \phi_{o_2}) - (\phi_{x_1} - \phi_{o_1}) \tag{4.7}$$

where ϕ_{x_2}, ϕ_{o_2}, ϕ_{x_1}, and ϕ_{o_1} are the true values of the phases. From calculations using electron-density profiles obtained from rocket data [*Edwards*, 1974b (Table 6.1)] it is expected that $\Delta\eta$ will lie between $-\pi$ and $+\pi$ up to about 83 km under active sun conditions and 85 km under quiet sun conditions, with $h_2 - h_1 = 1.5$ km. Thus, a multiple of 2π is added to the phase difference $\Delta\eta$ to obtain a value between $-\pi$ and $+\pi$.

Figure 4.1 shows two typical histograms of phase difference $\Delta\eta$, at 73.5 to 75 km, and 78 to 79.5 km. The data were collected near noon with a sample size of 5000. (The systematic variation between adjacent bins is due to the quantization error in the A/D converter and histogram bins.)

Histograms obtained from altitudes above 80 km are much broader than those displayed in Figure 4.1. This leads to an ambiguous determination of the phase angle, leading to large errors in the electron-density calculations at those altitudes. Similar results were reported by *Austin* [1971]. He attributed this effect to the different group velocities of the two propagating modes. The group velocities increasingly diverge as the difference between their refractive indices becomes larger with altitude. Austin defines an overlap function to describe the degree of overlap of the scattering volumes of the two modes. He finds that due to the group delay there is total overlap of scattering volumes up to about 86 km, and no overlap above 95 km. *Tanenbaum et al.* [1973a,b] made a study of phase-difference histograms and tried to fit them to histograms predicted by single-reflector and turbulence-volume models. They found that the observed data were in good agreement with both models, and could not predict the type of scattering. They also obtained phase-difference histograms which broadened with increasing altitude. They concluded that the broadening of the higher altitude phase-difference histograms was not necessarily due to nonoverlap of the scattering volumes, but due simply to the increasing difference between the differential phases of signals scattered from the top and bottom of the scattering volume.

Due to this broadening of the phase-difference histograms, reliable electron densities cannot be obtained above about 80 km. Two methods of extending the altitude range of the experiment would be to use a shorter pulse length or a higher operating frequency, both of which would limit the phase angle difference to smaller values.

4.2.2 *Data collection and processing programs.* The computer program used in collection of the differential-phase data is PCOLL. Listings of the

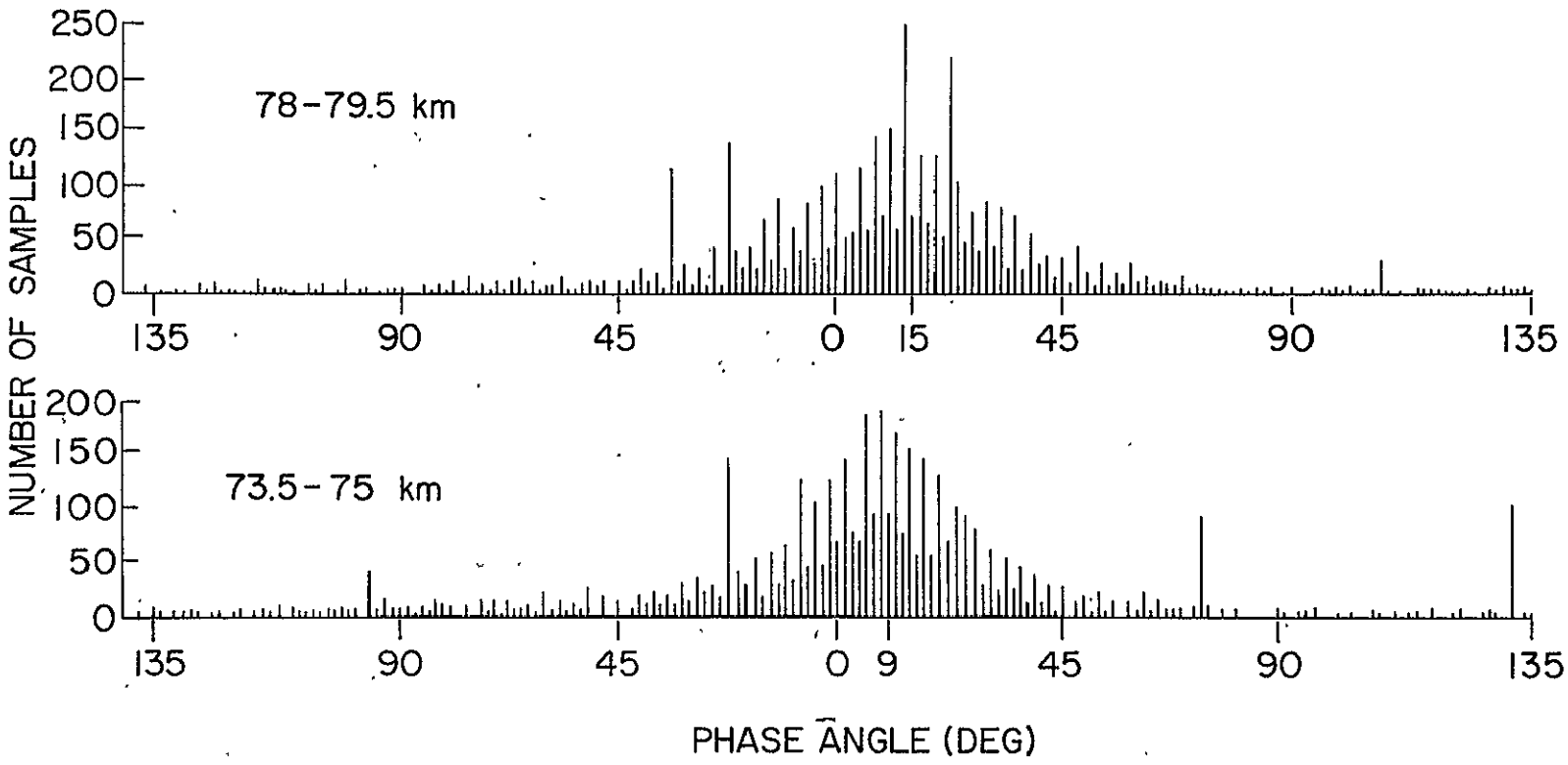

Figure 4.1 Histograms showing the distribution of the phase angle $(\phi_x-\phi_o)\big|_{h_2} - (\phi_x-\phi_o)\big|_{h_1}$ for the two altitudes, containing 5000 samples, observed on February 20, 1977 at 12:10. Each small division is 1.5 degrees.

program and all its subroutines are given in Appendix III. The subroutines are included in the partial-reflection program library (.LIBR5) and may be loaded automatically by the linking loader.

The program collects the data from the A/D converter and writes it in files onto a magnetic disk or DECtape. Provision is included to switch the system digital attenuator in to put any attenuation up to 63 dB ahead of the receiver to prevent its saturation. Normally, differential-absorption data are obtained first to obtain the attenuation necessary to prevent receiver saturation in the altitude range of interest. Data are stored in files of any length, as selected by the operator.

The phase angle processing and plotting program is PHIST, and is listed in Appendix III. The program reads the file of data written by PCOLL, calculates the phase difference $\Delta\eta$, adds or subtracts 2π to bring the phase angle into the range of $-\pi$ to $+\pi$, and plots the results in 1.5-degree increments.

The differential-phase electron-density profile calculation program is DPEX. This program and its many subroutines are also listed in Appendix III. DPEX reads the data file written by PCOLL and calculates the electron-density profile in the altitude range of 70.5 to 90 km. The program obtains a histogram of the phase difference $\Delta\eta$ at each pair of heights and finds the median of the distribution. This is called the first median. A 'second median' is obtained by taking the median of the distribution truncated at plus or minus 20 degrees from the first median. This is the phase difference $\Delta\eta$ used in the electron-density profile calculation. This 'second median' is used because it was found through experiment to be the best approximation to the center of the distribution of those methods tried. The electron densities are calculated using the full Sen-Wyller theory, by iteration in electron density. The profile calculation requires about five minutes of computation on the PDP-15/40 computer.

5. PARTIAL-REFLECTION ELECTRON-DENSITY MEASUREMENTS

In this chapter electron-density data analyzed by the methods described in Chapter 4 are presented.

5.1 *Daily Measurements of Electron Densities*

In order to identify the changes that occur in the *D*-region electron densities, data are collected on a daily basis at the Aeronomy Laboratory Field Station during the months of October through mid-April. Figures 5.1 through 5.7 are plots of the electron density at 72, 76.5, and 81 km, and the A_x/A_o ratio at 81 km for the months of October 1975 through April 1976. The A_x/A_o ratio, whose logarithm represents the total differential-absorption occurring below 81 km, gives an indication of the total electron density below 81 km. A high value of A_x/A_o at 81 km corresponds to a low total electron content below 81 km. The variations in electron density are relatively minor until the second week in November. Variability is greatly increased there, and the variability continues to grow larger until it maximizes in the month of February. This is clear evidence of the winter anomaly occurring at Urbana. Variability is again lowered by the second week in March, and continues at a low level through mid-April. When comparing plots of a particular altitude with plots of another altitude it can be seen that the electron densities at 72 and 76.5 km follow the same variational trends, suggesting a similar mechanism causing the changes at both altitudes. The 81-km electron densities are not as well correlated with those at the lower altitudes, suggesting that different mechanisms are causing the variation at 81 km. It can be seen though that when there is a sizeable peaking of electron density, it usually occurs at all altitudes. This suggests a mechanism that is large enough in consequence to disrupt the normal variations observed at each altitude.

Figure 5.8 is a plot of the electron density monthly means at 76.5 km. The electron densities are shown to be higher in the summer months as would be expected due to a smaller solar zenith angle in that period. Error bars indicating $\pm$ 1 standard deviation demonstrate the increased winter variability. The coefficient of variation (standard deviation/mean) is plotted in Figure 5.9 for electron densities at 72, 76.5, and 81 km. The increase in variability during the winter months associated with the winter anomaly is clearly shown. *Gregory and Manson* [1969b] did a similar analysis in the Southern Hemisphere and obtained results in agreement with those presented

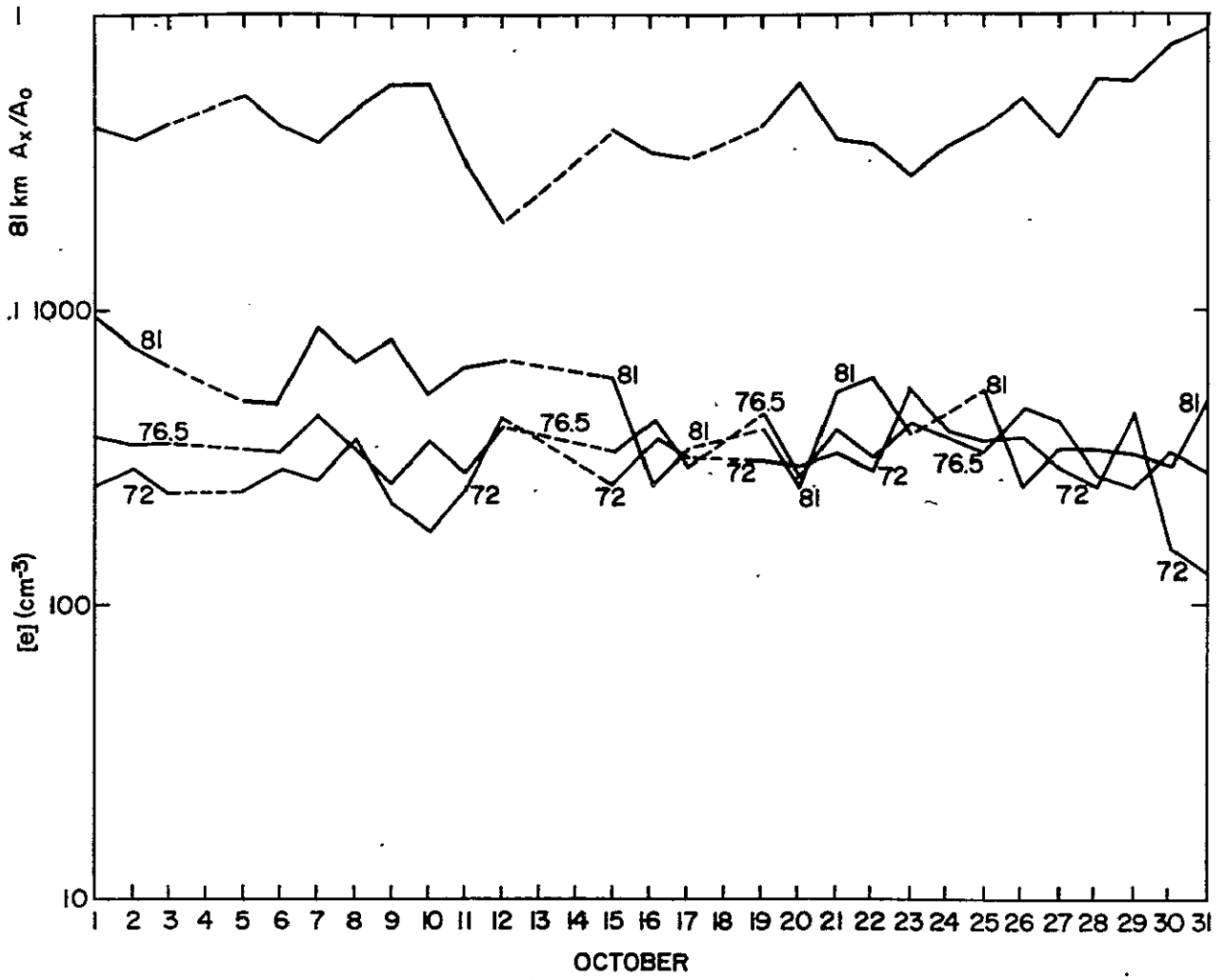

Figure 5.1 Daily plot of electron density at 72, 76.5, and 81 km and A_x/A_o at 81 km for October 1975.

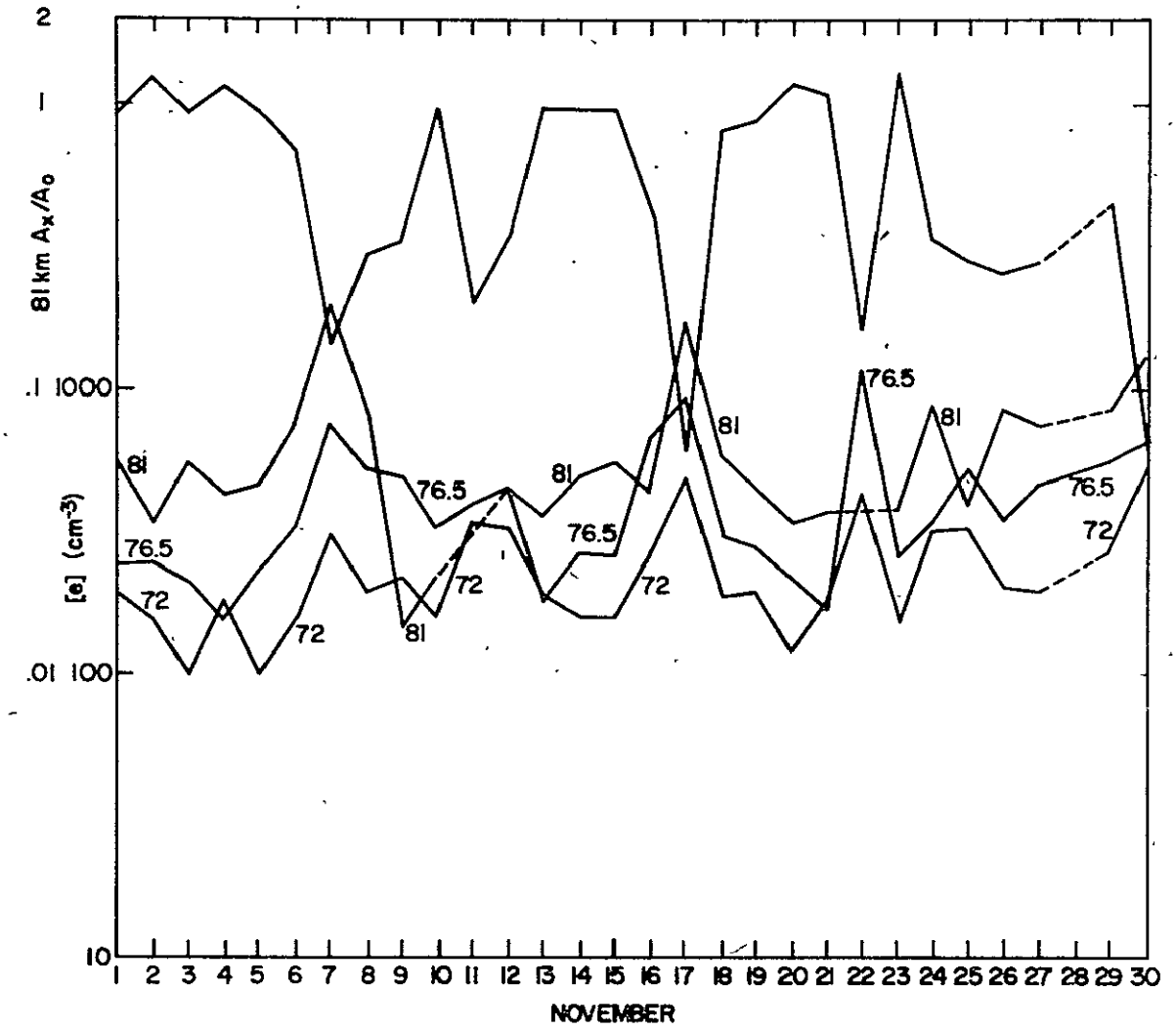

Figure 5.2 Daily plot of electron density at 72, 76.5, and 81 km and A_x/A_o at 81 km for November 1975.

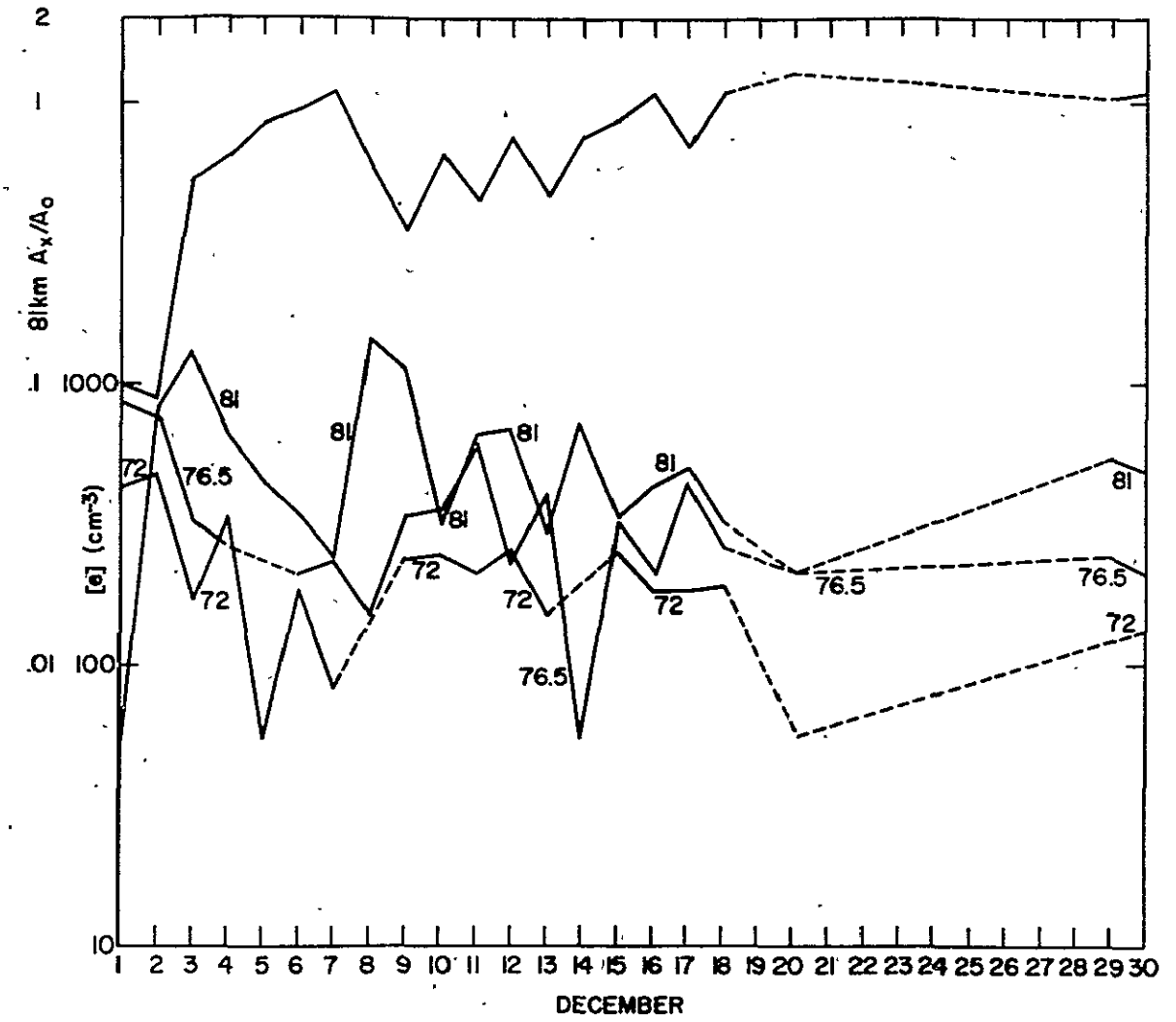

Figure 5.3 Daily plot of electron density at 72, 76.5, and 81 km and A_x/A_o at 81 km for December 1975.

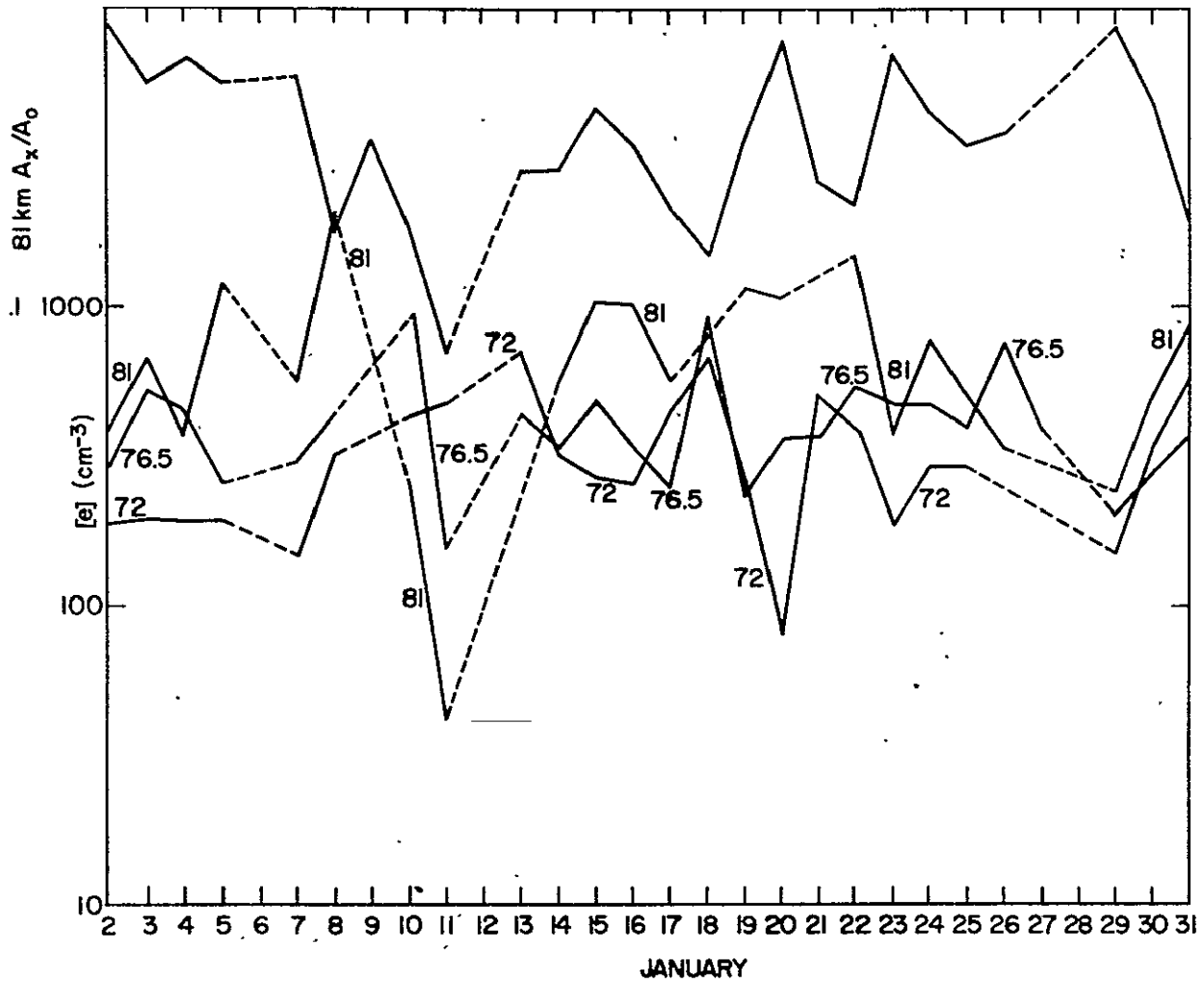

Figure 5.4 Daily plot of electron density at 72, 76.5, and 81 km and A_x/A_O at 81 km for January 1976.

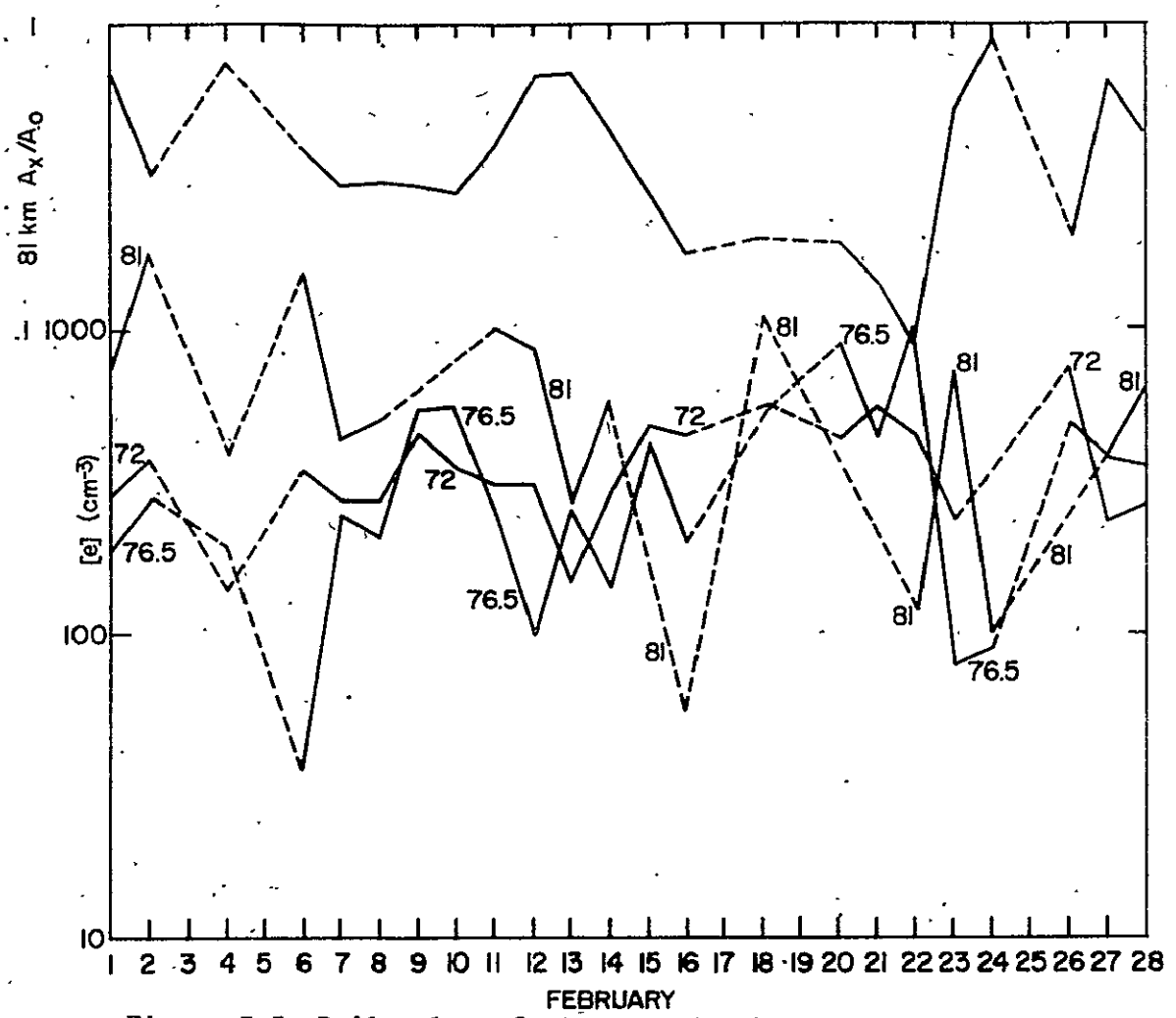

Figure 5.5 Daily plot of electron density at 72, 76.5, and 81 km and A_x/A_o at 81 km for February 1976.

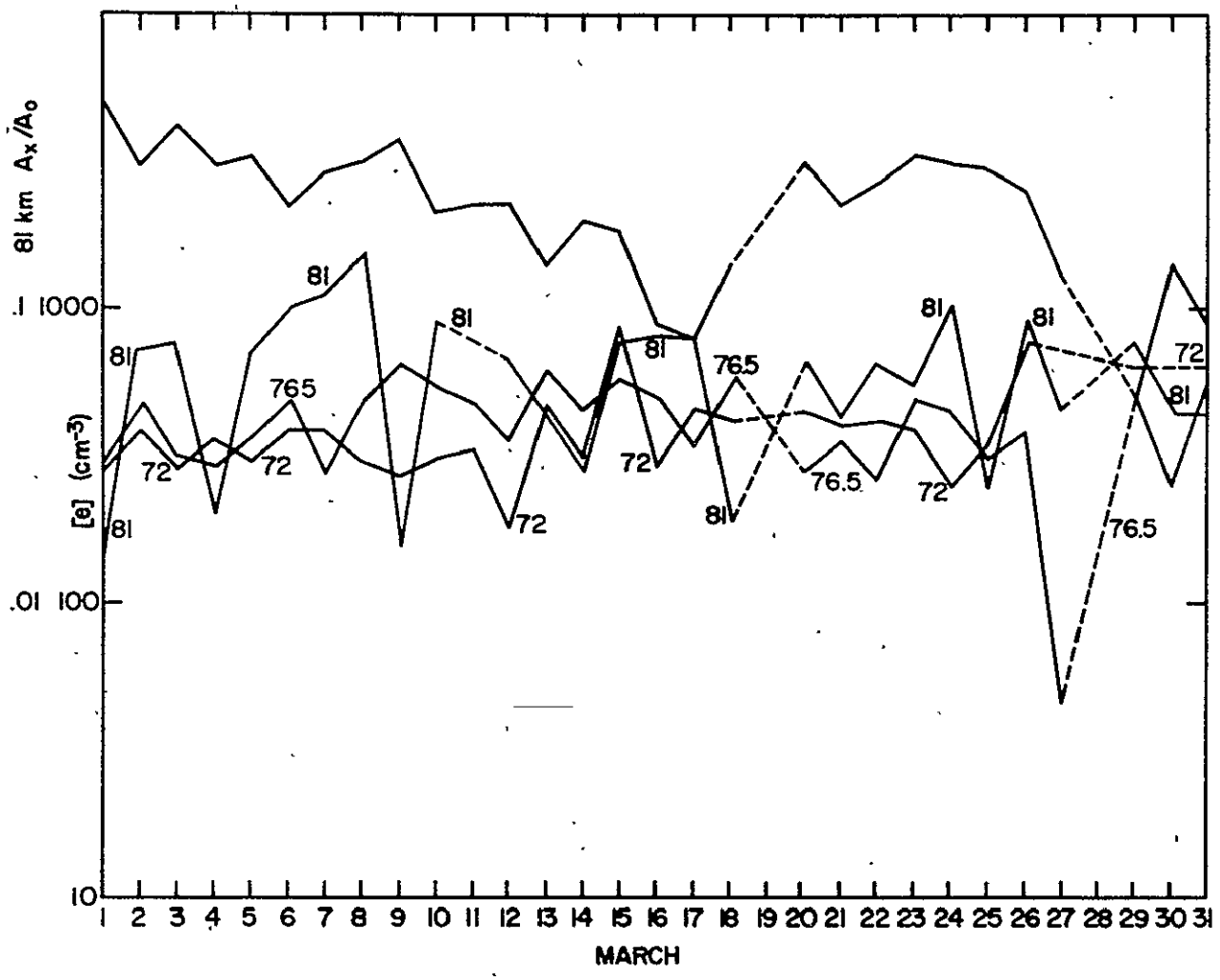

Figure 5.6 Daily plot of electron density at 72, 76.5, and 81 km and A_x/A_o at 81 km for March 1976.

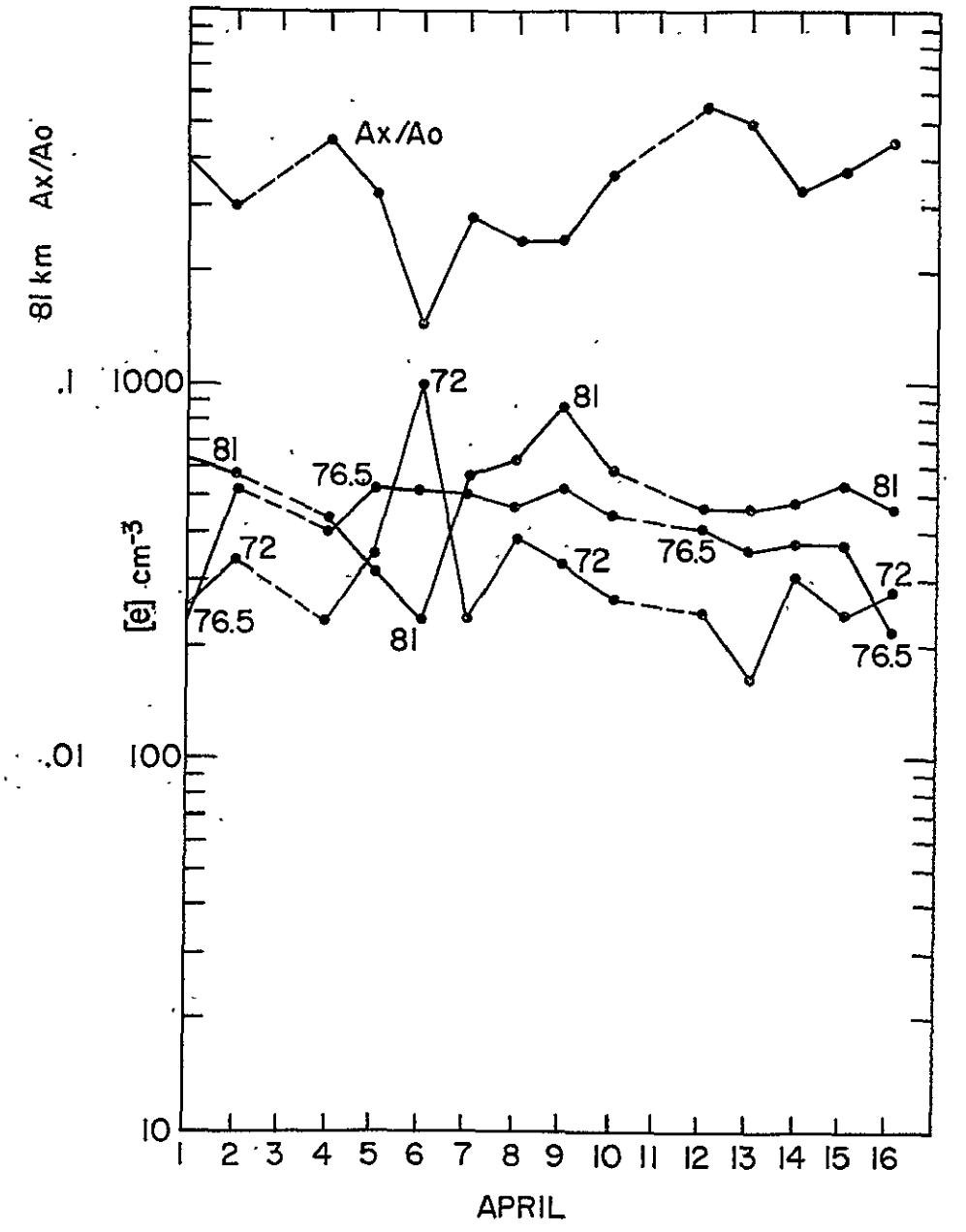

Figure 5.7 Da f electron density at 72, 76.5, and 81 km and A_x/A_o at 81 km for April 1976.

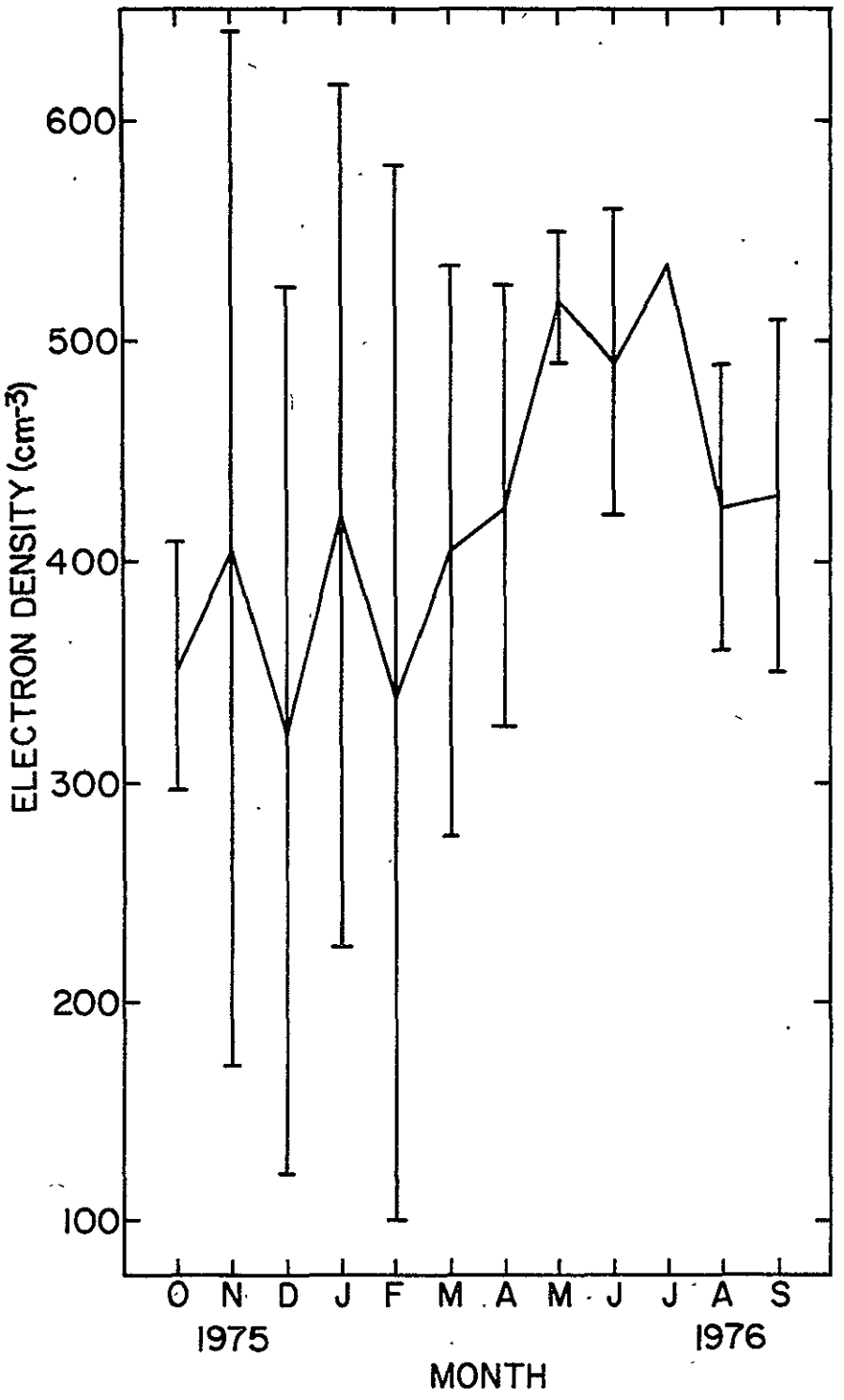

Figure 5.8 76.5-km electron-density monthly means. Error bars indicate ± 1 standard deviation.

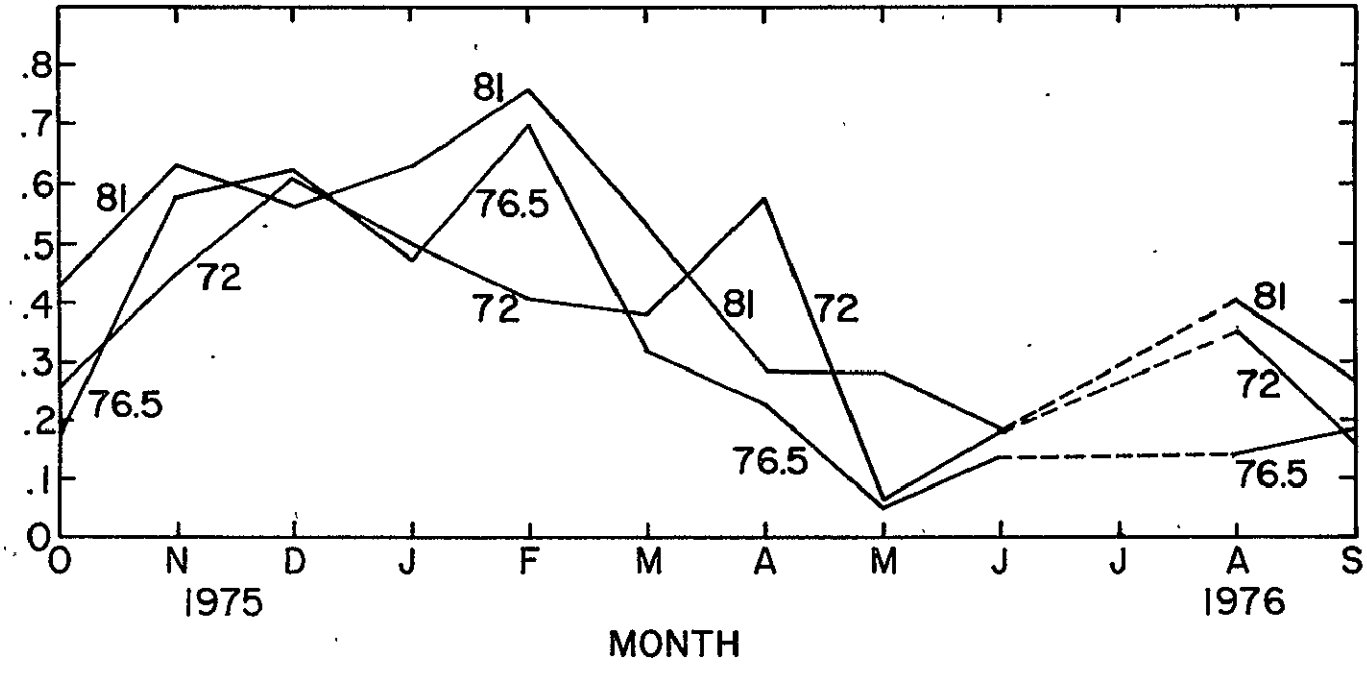

Figure 5.9 Coefficient of variation of electron densities at 72.0, 76.5, and 81.0 km.